NTNU

Norwegian University of
Science and Technology

A Method for Determining the Mode Shapes from a Finite Element Model for Use in a Finite-Mode Vibration Simulation Model

Thomas Gløersen Alm

Marine Technology
Submission date: January 2016
Supervisor: Eilif Pedersen, IMT

Norwegian University of Science and Technology
Department of Marine Technology

MASTER THESIS IN MARINE ENGINEERING

SPRING 2016

FOR

STUD.TECHN. Thomas Gløersen Alm

A METHOD FOR DETERMINING THE MODE-SHAPES FROM A FEM-MODEL FOR USE IN A FINITE-MODE VIBRATION SIMULTION MODEL.

Work description

Classical torsional vibration analysis of propulsion systems are well established and are carried out as a part of the classification of all ships. However, for some special cases it is require that time simulations are carried out. These cases are related to impulse loads on the power train, i.e. clutching, ice load on the propeller and especial non-linear effects. Time simulations relative to classical analysis requires a more detailed modelling of several of the components in the power train in addition to of cause the piston engine. Detailed engine models for process analysis are well established and combining these models would be of great interest for a more detailed analysis of marine power trains in these special cases.

The aim of this project is to investigate and possibly reformulate the torsional vibration problem for an engine crankshaft including a detailed description of the mechanism for transient analysis. The developed model should be easily coupled to engine process models in order to capture the cylinder pressure variations in time. The reduction of the crankshaft model should be carried out starting from a detailed finite element model or similar.

This project is both a continuation of previous research projects and part of ongoing Ph.d-projects at the Department

Scope of work:

1. Carry out a literature review on torsional vibration analysis and simulation and perform a critical assessment of the modelling and limitations of the analysis.

2. Develop a finite-mode model of the crankshaft for torsional simulations using the Lagrange-Hamiltonian/Bond Graph approach. Investigate the inclusion of the rigid-body crank mechanism into this model.

3. Using the FEM-software Abacus, shown how to extract vibration model parameters such as torsional inertia and stiffness for use in vibration simulation models.

4. Develop a methodology for how to extract the mode-shapes for the shaft from the finite element model. Demonstrate how the method on a simplified shaft model.

5. If time permits, assemble the assumed mode model using the parameters and mode-shapes obtained, devise relevant simulation cases and demonstrate the simulation properties and capabilities of such a model.

The report shall be written in English and edited as a research report including literature survey, description of mathematical models, description of control algorithms, simulations results, discussion and conclusion including a proposal for further work. Source code developed shall be provided on a CD or equivalent with code listing enclosed in appendix.

The Department of Marine Technology, NTNU, can use the results freely in its research work by referring to the students work.

The thesis should be submitted in three copies within 5 months after the registered start-up of this thesis.

Trondheim September, 2015

Eilif Pedersen
Associate Professor (Advisor)

Preface

The submission of this master's thesis marks the final step towards earning the degree of Master of Science at the Norwegian University of Science and Technology. The work on this thesis begun in September 2015 and ended in January 2016.

My interest in the field of vibration analysis arose when taking a course in mechanical vibrations in the spring of 2013. What appealed to me was the intersection between the challenging mathematical formulations that are used and the physical phenomena they describe. About a year later, I took a course in modelling and simulation of dynamic systems, in which I learned about the bond graph modelling language. The lessons from both these courses were used during this work.

The assignment required a fair amount of work using a finite element model in the computer program Abaqus. Having no background knowledge of the finite element method nor of finite element software, this proved to be very time-consuming. Fortunately, Ph.D. candidate Dražen Polić helped me along the way. I would like to offer my thanks to him for giving me good advice and ideas during this period.

I would also like to thank my advisor, associate professor Eilif Pedersen, for his valuable help during the work on this thesis.

Contents

List of Figures

List of Tables

Nomenclature

Roman letters

A	Area
A_n	Mode shape cofficient, mode shape n
a	Major semi-axis of ellipse; Time-varying velocity source
B_n	Mode shape cofficient, mode shape n
b	Minor semi-axis of ellipse
c	Damping coefficient
c_{cr}	Critical damping coefficient
D	Dissipative energy
d	Radial distance to axis of rotation (for use in parallel axis theorem)
E	Young's modulus of elasticity
e'	Displacement derivative of the Lagrangian
F	Applied force
f	Frequency
G	Shear modulus
g	Gravitational acceleration
I	Mass moment of inertia
J	Polar second moment of area
K_t	Carter's formula stiffness; Ker Wilson's formula stiffness
k	Rotational stiffness, translational stiffness
L	Length; Lagrangian, $L = T - V$
l	Connecting rod length
M	Symmetric $N \times N$ mass matrix
m	Mass
N	Number of generalized coordinates
p	Momentum
Q	Generalized force
q	Displacement; Generalized coordinate
r	Radius; Crank radius
r_{con}	Distance from gudgeon pin to connecting rod's center of mass
T	Kinetic energy; Torque
U	Modal displacement value calculated numerically
V	Potential energy
Y_n	nth mode shape function

Greek letters

γ	Angle between connecting rod and y-axis
ζ	Dimensionless damping ratio
η_n	nth modal displacement
θ	Angular displacement of crankshaft
$\Delta\theta$	Ignition angle
λ	Connecting rod ratio
ν	Poisson's ratio
ξ	Longitudinal displacement of vibrating bar
ρ	Mass density
ω	Natural frequency

Abbreviations

TVD	Torsional vibration damper
CAD	Computer-aided design
FEM	Finite element method
MJ	Main journal
CW	Crank web
CP	Crank pin
CM	Crank mechanism

Abstract

In this thesis, a methodology for retrieving mathematical expressions of the mode shapes of a crankshaft based on numerical data yielded by a finite element model is presented and tested. The mode functions should be used as inputs to a finite-mode bond graph model of a crankshaft.

The contents and results of two papers related to torsional vibration modelling and simulation were presented, and their relevancy to this work was briefly discussed. A relevant section from a book on bond graph modelling was also presented. This section described an approach called finite-mode bond graph modelling, in which a continuous dynamic system is reduced to a modal representation. In order for this approach to work, the mode shapes of the system must be orthogonal.

A finite-mode IC-field bond graph representation of the crankshaft and crank mechanism were made using the Lagrange-Hamiltonian approach. However, this bond graph required the value of the mode shapes at the locations of torque input. These mode shapes were to be obtained from finite element models.

Models of a simple shaft and a single crank throw were made in the finite element software Abaqus. To check that the models were made correctly and to gain some experience with the software, the inertia and stiffness parameters were also retrieved. They were found to match their analytical counterparts well.

A frequency analysis was conducted in order to obtain the natural frequencies and corresponding mode shapes. The modal displacements at different locations along the axial direction were exported into a spreadsheet and plotted. From these numerical values, a set three of equations were set up to obtain a mathematical expression for each mode shape.

First a verification of the methodology was conducted on the simple shaft, as its analytical mode shapes and natural frequencies are well-known. The method worked well for this simple model. The resulting mathematical expressions for each mode shape were very close to the analytical form.

For the single crank throw, the overall shape of the numerical mode shapes and their corresponding mathematical expressions matched well. However, there was a considerable spread between the displacement values. More-

over, the obtained mathematical mode shapes were non-orthogonal, which meant that they couldn't be used in the finite-mode bond graph model of the crankshaft.

Another attempt was made at probing a different set of nodes from which the mathematical mode shape expressions could be obtained. However, the resulting mode shape expressions still turned out to be non-orthogonal.

The mathematical mode shape expressions could possibly fit the numerical points better if more than three equations were used. However, the problem could also be the manner in which the numerical values were obtained from the finite element model.

No simulations were run on the bond graph model. If a method is found to obtain orthogonal mode shapes for the crankshaft, the bond graph can get its required inputs. Simulations should then be run to verify its validity. The model could also be connected to existing models of a marine propulsion system.

Sammendrag

I denne oppgaven presenteres en metode for å hente ut matematiske uttrykk for egensvingeformene til en veivaksel basert på numeriske data fra en elementmetodemodell. Hensikten er at egensvingeformene skal brukes som inndata i en modal båndgraf-modell av veivakselen.

Innhold og resultater fra to artikler angående modellering og simulering av torsjonsvibrasjoner ble presentert, og deres relevans i forhold til denne oppgaven ble kort diskutert. Et relevant kapittel fra en bok om båndgrafmodellering ble også presentert. I denne delen beskrives en metode for modal båndgraf-modellering, hvor et kontinuerlig dynamisk system reduseres til en modal representasjon. For at denne metoden skal fungere, må egensvingeformene til systemet være ortogonale.

En modal IC-felt båndgraf-representasjon av veivakselen og veivmekanismen ble laget ved bruk av Lagrange-Hamiltons tilnærming. Denne modellen krevde imidlertid egensvingeformenes verdier ved punktene der dreiemomentet påføres. Disse egensvingeformene skulle hentes fra elementmetodemodeller.

Modeller av en enkel aksling og ei enkel veiv ble laget i elementmetodeprogramvaren Abaqus. For å sjekke at modellen var blitt laget på riktig måte, og for å få litt erfaring med programvaren, ble massetreghetsmoment og stivhetsparametre også hentet ut. De viste seg å stemme godt overens med analytiske resultater.

En frekvensanalyse ble utført for å skaffe modellenes egenfrekvenser og korresponderende egensvingeformer. De modale forskyvningene på ulike steder i den aksielle retningen ble eksportert til et regneark og plottet. Fra disse numeriske verdiene ble et ligningssett på tre ligninger med tre ukjente satt opp for hver egensvingeform. Fra disse kunne et matematisk uttrykk for egensvingeformen bli funnet.

Først ble metoden verifisert ved bruk av modellen av den enkle akslingen, siden de analytiske egenfrekvensene og egensvingeformene for en slik modell er velkjente. Metoden fungerte bra for denne enkle modellen; de resulterende matematiske uttrykkene for hver egensvingeform var meget nære den analytiske løsningen.

For den enkelte veiva passet den generelle fasongen til de numeriske egensvinge-

formene godt til de matematiske uttrykkene. Det var imidlertid en betydelig spredning mellom forskyvningsverdiene. Videre ble det funnet at de matematiske egensvingeformuttrykkene ikke var ortogonale, noe som medførte at de ikke kunne brukes i den modale båndgraf-modellen av veivakselen.

Et nytt forsøk ble gjort der forskyvningene for et annet sett noder ble hentet ut, og et nytt sett matematiske uttrykk for egensvingeformene ble laget. Disse viste seg å heller ikke være ortogonale.

De matematiske uttrykkene for egensvingeformene kunne muligens passet de numeriske punktene bedre dersom flere enn tre ligninger ble anvendt. Problemet kan imidlertid også ligge i hvordan de numeriske verdiene hentes fra elementmetodemodellen.

Ingen simuleringer av båndgraf-modellen ble gjort. Hvis en metode blir funnet som produserer ortogonale egensvingeformer for veivakselen, kan båndgraf-modellen få de nødvendige inndata. Det bør deretter kjøres simuleringer av modellen for å bekrefte dens gyldighet. Modellen kan også kobles til eksisterende modeller av et marint fremdriftssystem.

CHAPTER 1

Introduction

Before tackling the task of modelling a crankshaft system, some background knowledge should be obtained. Two papers related to torsional vibration modelling and simulation will be reviewed, and the potential shortcomings of the methods used will be discussed. A relevant section of a book on bond graph modelling will also be included. In that section, a finite-mode bond graph modelling procedure for a longitudinally vibrating bar is presented. This procedure will later be applied to model a crank throw.

Next, more theory for creating the bond graph models of a crankshaft will be presented. This is followed by a description of the steps taken towards creating these models. More specifically, the development of models of a single crank throw and its corresponding crank mechanism is shown. The model of the single crank throw will be a modal representation, and the crank mechanism will be modelled using the Lagrange-Hamiltonian approach. This results in an IC field representation of the crank mechanism and the crank throw.

The finite element analysis program Abaqus will be used to extract natural frequencies and mode shapes. A method to convert the numerical modal displacement values given by Abaqus to mathematical mode shape expressions will be presented. A finite element model of a simple shaft is created and used to verify the validity of this method.

The method will then be applied to a finite element model of a single crank throw based on an existing model of the entire crankshaft. The procedure for creating the crank throw model is explained, and the results of numerical estimations of mass and stiffness and of a frequency analysis will be presented. The mathematical mode shape expressions yielded by the conversion method are to be used in the finite-mode bond graph model.

Finally, some concluding remarks and suggestions for further work will be made.

CHAPTER 2

Literature Review

Before creating the model, a literature review should be carried out. The objective is to get familiar with existing methods of torsional vibration modelling. An overview of the methods used and results obtained from each article is presented, and a brief remark on the relevance to this thesis will be given.

Please note that all results and conclusions in this section are obtained and reached by the authors of the respective papers cited at the start of each subsection.

2.1 Analysis of torsional vibration in internal combustion engines: modelling and experimental validation

2.1.1 Overview of the work

In this paper, Mendes et al. (2008) study the torsional vibrations of a crankshaft in an internal combustion engine. Two mathematical models of the crankshaft were made using the lumped mass approach: One considering a single mass viscous torsional vibration damper (TVD) (figure 2.1), and one considering a double mass rubber TVD (figure 2.2).

The inertias were determined by use of a computer-aided design (CAD) program, while the stiffnesses were calculated using finite element models for the crankshaft model and the rubber TVD. The stiffness of the viscous TVD was found using a methodology given in Wakabayashi et al. (1992) and empirical data. The system's relative damping coefficients were obtained from the loss angle property. The excitation torque for each cylinder was found by multiplying the resulting tangential force on the crank throw by the crank radius. The resulting tangential force was found to be a vector sum of the tangential combustion gas load and the tangential inertial force. The inertia, damping and stiffness matrices were derived, and the resulting tangential forces for each cylinder were put into an excitation torque vector. Because the elements of this vector consisted of periodically exciting torques, a finite Fourier series was used to solve the system. Next, the dynamics of the crankshaft

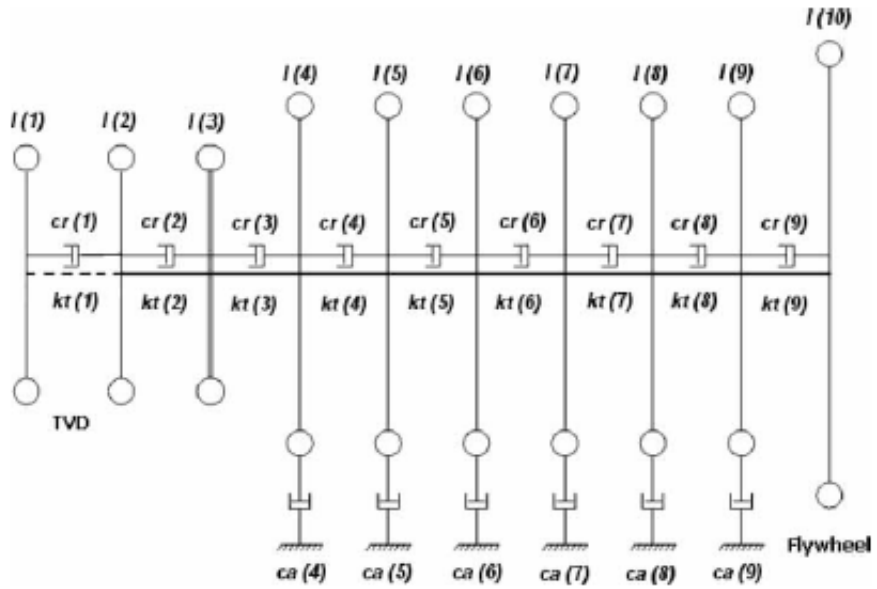

Figure 2.1: Lumped mass model of the crankshaft system with 10 inertias – Retrieved from Mendes et al. (2008)

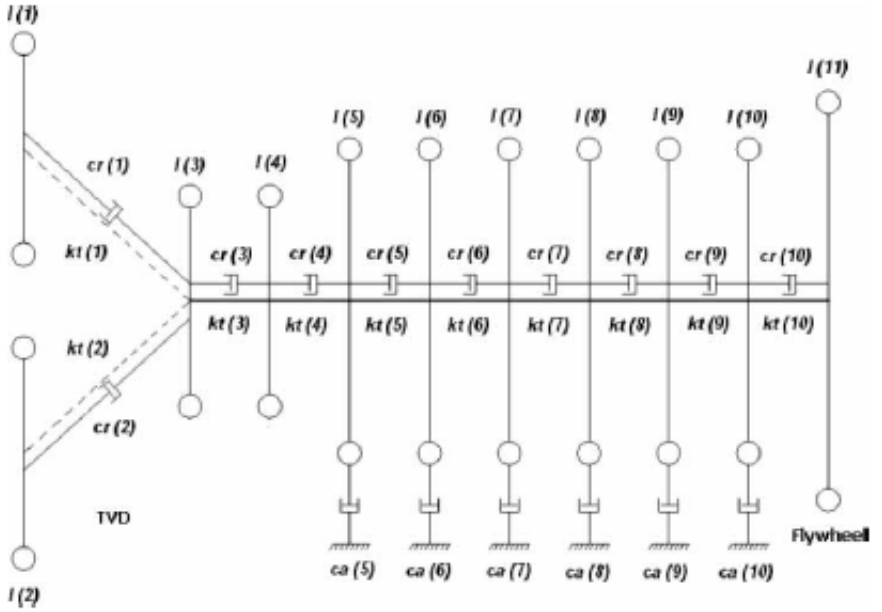

Figure 2.2: Lumped mass model of the crankshaft system with 11 inertias – Retrieved from Mendes et al. (2008)

system were written as a first-order differential state equation. This equation was then solved using the transition state matrix and the convolution integral. Further, expressions for calculating the dissipated energy in the rubber TVD and viscous TVD were given along with permissible parameters.

2.1.2 Results and conclusions

In order to verify the mathematical models, experimental measurements of the crankshaft were carried out. Simulations of the mathematical model of the crankshaft system with and without TVDs were carried out and compared to the measured results. Due to the similarity of the results, Mendes et al. (2008) concluded that the method for creating the equivalent mathematical model and the hypotheses upon which it is made are valid. Graphs of the calculated and measured torsional vibration amplitudes in the crankshaft pulley with a viscous damper are shown in figure 2.3 and 2.4 respectively.

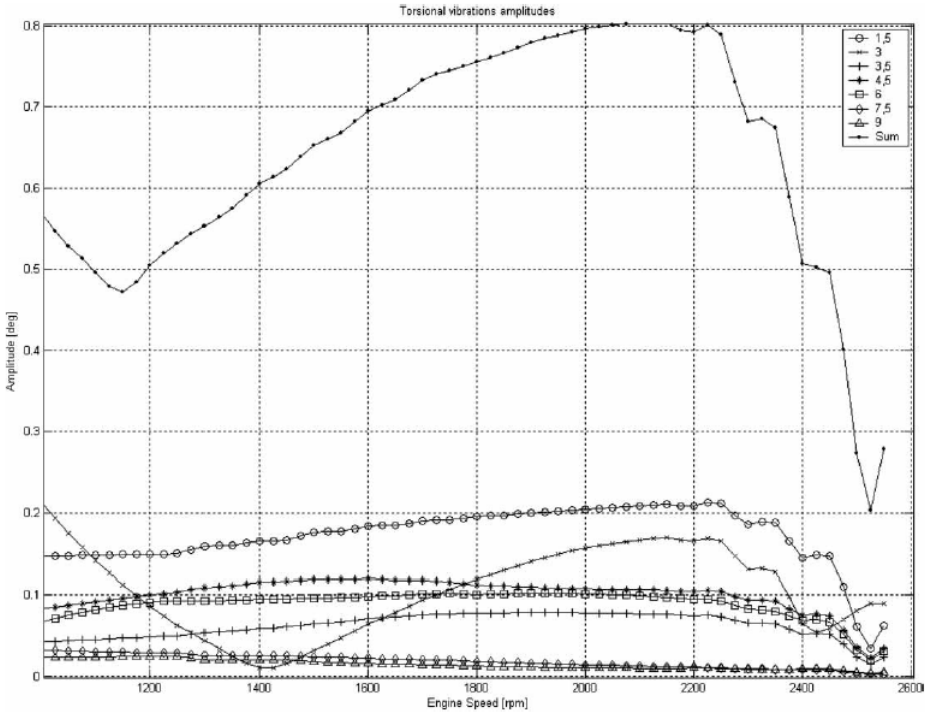

Figure 2.3: Calculated torsional vibration amplitudes of different orders – Retrieved from Mendes et al. (2008)

However, Mendes et al. (2008) pointed out that the methodology might not be suitable for internal combustion engines with larger displacement, as the

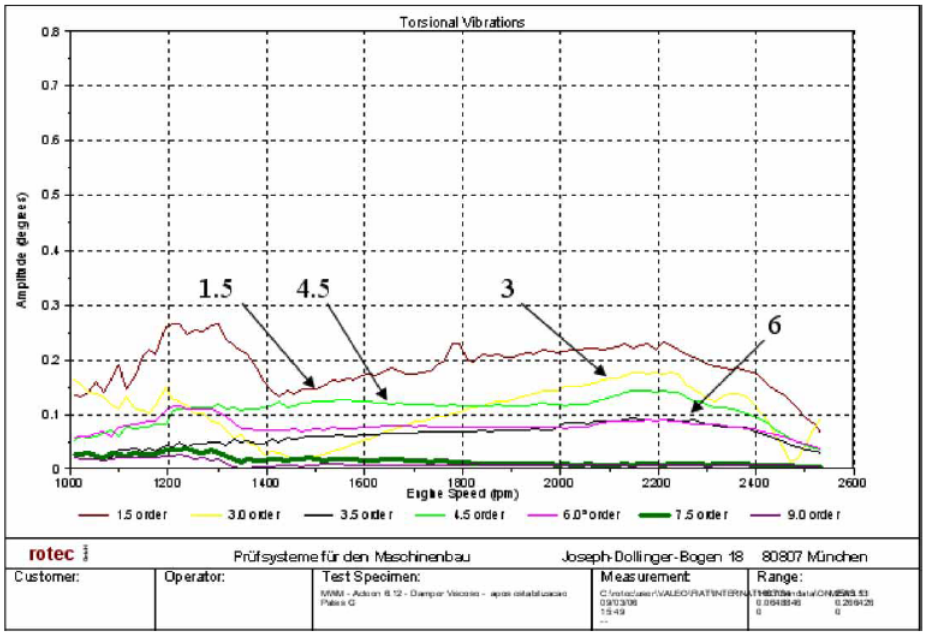

Figure 2.4: Measured torsional vibration amplitudes of different orders – Retrieved from Mendes et al. (2008)

effect of e.g. axial vibrations will be too significant to neglect.

2.1.3 Relevance to this master's thesis

The focus of this paper is on comparing the results of a mathematical model of the torsional vibrations with experimental results. The secondary focus is on dimensioning and choice of a torsional vibration damper. Modal analysis and model reduction was not considered, nor was bond graph modelling. The methodology for retrieving parameters such as inertia, damping and stiffness was well presented. The methodology for determining the inertias was different from what will be used in this thesis, as the authors used CAD software. The stiffness was retrieved using a finite element model, which will be done in this thesis.

2.2 Non-linear Torsional Vibration Characteristics of an Internal Combustion Engine Crankshaft Assembly

2.2.1 Overview of the work

In this paper, Huang et al. (2012) studied the non-linear torsional vibrations of a crankshaft in an internal combustion engine. First, a lumped mass model called "the non-constant inertia model" was made. It is shown in figure 2.5.

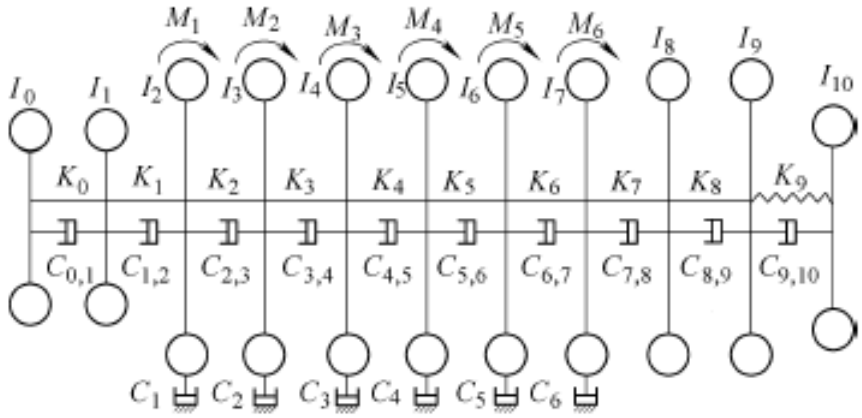

Figure 2.5: Lumped mass model of the crankshaft system – Retrieved from Huang et al. (2012)

Next, an expression for the instantaneous inertia (also called non-constant inertia), i.e. the inertia as a function of crank angle θ, of a single cylinder was derived. The result was used to express the kinetic energy, T. The potential energy, V, and the dissipative energy, D, were also derived for use in the Lagrange equation. Both the internal and external excitation torques were derived. Huang et al. (2012) found that the internal excitation torque arises from the non-constant inertia, while the external excitation torque comes from the combustion process in the cylinder and the reciprocating inertia. A fast Fourier transform was applied to the external torque, and an expression for the harmonic torque of the cylinders was found. Both a free and forced vibration analysis were done, and the resulting mode shapes and angular displacements were investigated for the different models.

2.2.2 Results and conclusions

For the lumped mass model, only the first four modes were found to be relatively accurate. Of these, the first two could be ignored (Huang et al. (2012)).

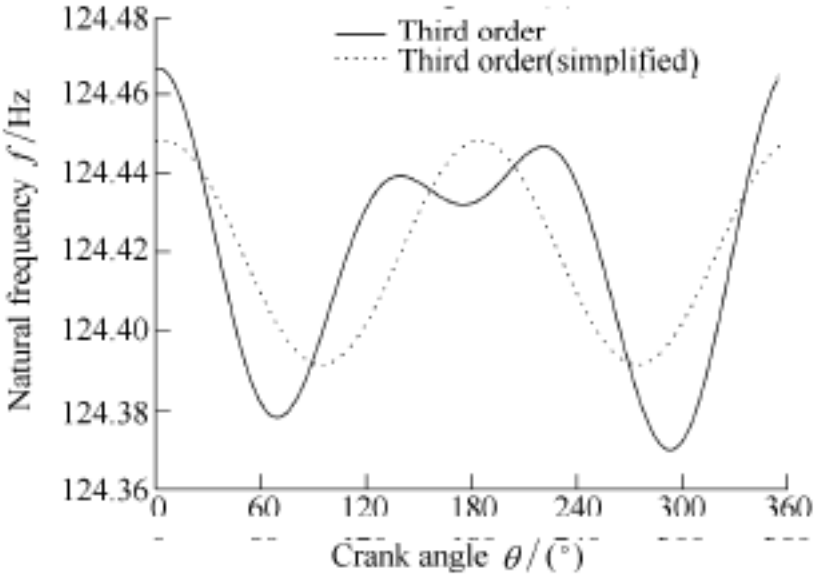

Figure 2.6: Natural frequencies for the precise and simplified equations – Retrieved from Huang et al. (2012)

A graph of the third order natural frequencies yielded by using the precise and simplified equations is shown in figure 2.6. The "precise equation" is the aforementioned instantaneous inertia. The "simplified equation" was derived by assuming that some of the terms of the precise equation can be neglected. Huang et al. (2012) found that the natural frequency varies with the crank angle due to the instantaneous inertia. Therefore, critical speeds are given as frequency ranges that grow with harmonic orders. An error of less than 1 % was found when comparing the natural frequencies calculated by the simplified and precise equations, so the simplified inertia equation was deemed to provide sufficient precision. Further, the four different dynamic models yield similar natural frequencies with a maximum error of 3 %. A finite element model was created in the computer program ANSYS and an analysis of the mode shapes was done. The resulting frequencies yielded by ANSYS agreed well with the ones already calculated.

In the forced vibration analysis, the torque contributions from the non-constant inertia and external torque were included in the dynamic equations

of the crankshaft system. Huang et al. (2012) found that an increase in engine speed leads to a decrease in the angular displacement amplitude of torsional vibrations. Further, the second order rolling vibration was found to be a result of the additional torque introduced by the non-constant inertia. It was also found that the non-constant inertia provides a damping torque proportional to the engine speed squared, which causes the system response to go through periodic, quasi-periodic and chaotic motion with increasing engine speed. Larger reciprocating inertia torque and smaller combustion gas torque were found to give the least rolling vibration at low harmonic orders, while the torsional vibration generally increased. Comparisons of the simulations of the different models were done. All the simulations showed that the 3rd order amplitude was the greatest. Huang et al. (2012) noted that the non-constant inertia model gave the lowest amplitude due to the damping torque provided by the non-constant inertia. The amplitude of the lumped mass model was found to be larger than in the detailed model, since the lumped mass model doesn't account for the internal damping of the shaft. Further, at orders larger than 7, the non-constant inertia model was found to produce a much higher angular displacement amplitude than the constant inertia models. Huang et al. (2012) explain that this is due to the the additional torque and the widened critical speed zones.

2.2.3 Relevance to this master's thesis

Model reduction was not performed in this paper, neither was bond graph modelling. However, the detailed expression for non-constant inertia can potentially be used in the work on this thesis. The Lagrange rule was also used to develop the equations of motion, which is similar to what will be done in this thesis. A finite element model was also used, but not in the same software as used in this work nor towards the same goal.

2.3 Finite-mode bond graph modelling

In this section of Karnopp et al. (2012), separation of variables is used to create a finite-mode bond graph representation of a continuous vibrating bar. The basis of the method is the partial differential equation for forced longitudinal vibration of a bar:

$$\rho\frac{\partial^2\xi}{\partial t^2} - E\frac{\partial^2\xi}{\partial x^2} = \frac{F(t)}{A}\delta(x-L) \tag{2.1}$$

where ρ is the density of the bar, ξ is the displacement of the bar, E is the Young's modulus, A is the cross-sectional area of the bar, and $\delta(x - L)$ is the Dirac delta function.

The external force $F(t)$ is set to zero and separation of variables is used to find a solution consisting of two functions: One depending on the x position of the bar, and one depending on time. These are denoted $Y(x)$ and $f(t)$.

Karnopp et al. (2012) substitutes $Y(x)$ and $f(t)$ in 2.1, solves the resulting ordinary differential equations and finds n distinct solutions. This means that there are n functions depending on x, $Y_n(x)$, called mode shapes. These mode shapes are on the form

$$Y_n(x) = A_n \cos(\alpha_n x) + B_n \sin(\alpha_n x) \tag{2.2}$$

where each α_n has a corresponding natural frequency ω_n.

In the case of the vibrating bar, Karnopp et al. (2012) points out that the mode shapes are orthogonal. This means that they have the following property (Meirovitch (1967)):

$$\int_0^L Y_n(x) Y_m(x) dx \begin{cases} = 0 \ , & n \neq m \\ \neq 0 \ , & n = m \end{cases} \tag{2.3}$$

Karnopp et al. (2012) points out that the solution to equation 2.1 can be written as:

$$\xi(x,t) = \sum_{n=1}^{\infty} Y_n(x) \eta_n(t) \tag{2.4}$$

where $Y_n(x)$ is the nth mode shape and $\eta_n(t)$ is the nth modal coordinate. This expression holds for both the forced and unforced case.

Karnopp et al. (2012) substitutes equation 2.4 in equation 2.1, multiplies each term by the mth mode shape Y_m, then applies the orthogonality property of the mode shapes described in equation 2.3. The approach is described in its entirety in section 10.2 of Karnopp et al. (2012). In short, it is found that equation 2.1 can be rewritten in terms of modal momentum, $p_m = m_m \dot{\eta}_m$, and modal displacement, $q_m = \eta_m$:

$$\frac{d}{dt} p_m = -k_m q_m + F(t) Y_m(L) \tag{2.5}$$

$F(t)$ is the external force, $k_m = m_m\omega_m^2$ is the mth modal stiffness, ω_m is the mth natural frequency, and m_m is the mth modal mass given by:

$$m_m = \int_0^L \rho A Y_m(x)^2 \, dx \tag{2.6}$$

Karnopp et al. (2012) combines equation 2.4 with the fact that $q_m = \eta_m$, $\dot{q}_m = p_m/m_m$, and multiplies each side with $F(t)$:

$$F(t)\frac{\partial \xi(L,t)}{\partial t} = \sum_{m=1}^{\infty} F(t) Y_m(L)\dot{\eta}_m(t) \tag{2.7}$$

This expression is shown in bond graph notation in figure 2.7

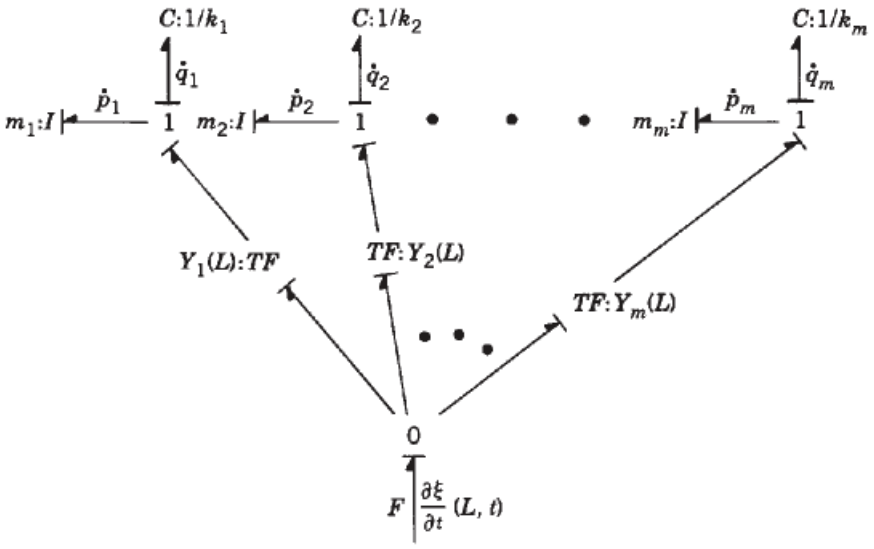

Figure 2.7: Bond graph of equation 2.7 – Retrieved from Karnopp et al. (2012)

Karnopp et al. (2012) also shows that it is possible to retrieve the response at more than one point in the system. In that case, the bond graph will take the form shown in figure 2.8:

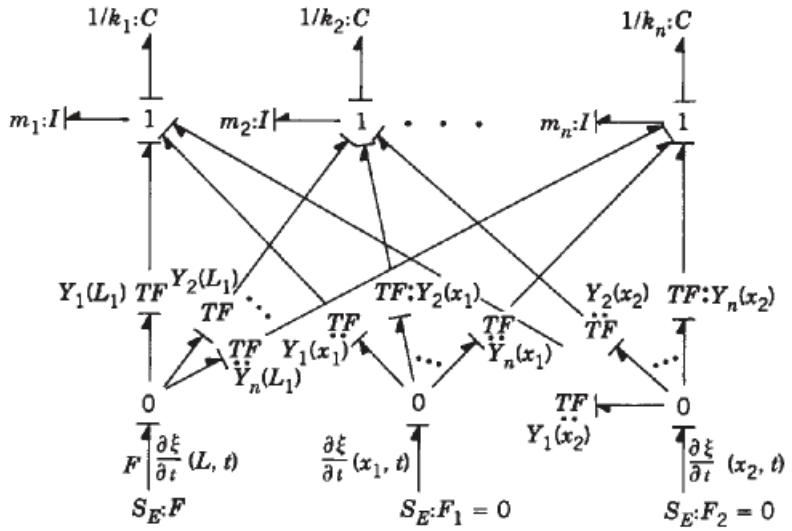

Figure 2.8: Modal bond graph model with multiple force inputs – Retrieved from Karnopp et al. (2012)

CHAPTER 3

Theory

In this section, the necessary theoretical material for developing the bond graph model of the crankshaft will be described. A short presentation of the bond graph modeling method will also be given. The method of modelling an IC-field using the Lagrange-Hamiltonian approach will also be included.

3.1 Lagrange's equations and the equations of motion

Lagrange's equations can be derived directly from Newton's laws. They are given as (Ginsberg (1998)):

$$\frac{d}{dt}\left(\frac{\partial T}{\partial \dot{q}_j}\right) - \frac{\partial T}{\partial q_j} + \frac{\partial V}{\partial q_j} = Q_j, \qquad j = 1, 2, \ldots, n \tag{3.1}$$

where T is the kinetic energy, V is the potential energy, Q_j is the jth generalized force and q_j is the jth generalized coordinate. The kinetic and potential energy are:

$$T = \sum_{j=1}^{N} \frac{1}{2} I_j \dot{q}_j^2 \tag{3.2}$$

and

$$V = \sum_{j=1}^{N} \frac{1}{2} k_j q_j^2 \tag{3.3}$$

where I_j is the jth moment of inertia and k_j is the jth stiffness. I_j can be given in either kg (translation) or $kg \cdot m^2$ (rotation), and k_j can be given in either N/m (translation) or Nm/rad (rotation).

As equation 3.1 shows, the kinetic energy is differentiated with respect to each generalized coordinate and its time derivative. The potential energy is differentiated with respect to each generalized coordinate.

A term for the dissipative energy D can also be included:

$$D = \frac{1}{2} c_j \dot{q}_j^2, \quad j = 1, 2, \ldots, n \tag{3.4}$$

where c_j is the jth damping coefficient. c_j can be written as (Pedersen and Valland (2014)):

$$c_j = 2\zeta_j I_j \omega_{n,j} \tag{3.5}$$

where $\omega_{n,j}$ is the jth natural frequency and ζ_j is the jth dimensionless damping ratio given by

$$\zeta_j = \frac{c_j}{c_{cr,j}} \tag{3.6}$$

where $c_{cr,j} = 2\sqrt{k_j \cdot I_j}$ is the jth critical damping coefficient.

If the dissipative energy is included, it is differentiated with respect to the time derivative of the generalized coordinate and added to the left side of equation 3.1.

The generalized force Q_j will, in the case of a crankshaft, be the force applied at the crank position, creating a torque $T(t)$ about the axis of the main journal. This force arises from the combustion gas pressure in the cylinder acting on the piston. The force acting on the piston is transferred through the connecting rod, which in turn acts on the crank to convert a translational motion to a rotational motion.

When Lagrange's equations are used, the equations of motion for the system are obtained. In the case of a crankshaft, a natural choice of generalized coordinate q would be the crank angle θ. In matrix and vector form, the equations of motion can thus be written as (matrices are in brackets and vectors are boldface):

$$[I]\ddot{\boldsymbol{\theta}} + [C]\dot{\boldsymbol{\theta}} + [K]\boldsymbol{\theta} = \mathbf{T}(t) \tag{3.7}$$

3.2 Mass moment of inertia

The moment of inertia of a rigid body rotating about the z-axis is defined as (Ginsberg (1998)):

$$I_{zz} = \iiint (x^2 + y^2) dm \tag{3.8}$$

For a shaft, the moment of inertia is:

$$I_{zz,cylinder} = \frac{1}{2} \overbrace{\rho \pi r^2 L}^{\text{Mass}} r^2 \tag{3.9}$$

where r and L are the radius and length of the shaft respectively. For an elliptical cross section, it is:

$$I_{zz,ellipse} = \frac{1}{4} \overbrace{\rho \pi a b L}^{\text{Mass}} (a^2 + b^2) \tag{3.10}$$

where a and b are the major and minor semi-axes respectively.

If the body's local axis of rotation is at a radial distance d from the actual axis of rotation, the parallel axis theorem must be used (Ginsberg (1998)):

$$I_{zz} = I_{body} + m_{body} d^2 \tag{3.11}$$

3.3 Rotational stiffness

The rotational stiffness, k, is defined as the ratio between applied torque, T, and angular displacement, θ, due to that torque (Friswell et al. (2012)):

$$k = \frac{T}{\theta} = \frac{GJ}{L} \tag{3.12}$$

where G is the shear modulus of the material, L is the length of the shaft, and J is the polar second moment of area given by:

$$J = \int_A r^2 dA \tag{3.13}$$

where A is the cross sectional area and r is the distance to the rotation axis.

G is related to the Young's modulus E by (Irgens (1999)):

$$G = \frac{E}{2(1+\nu)}$$

where ν is the Poisson's ratio for the material.

The final part of equation 3.12 is only accurate for circular cross sections, e.g. a shaft. For other cross sections, J can be multiplied by a correction factor, or a finite element analysis can be done instead (Friswell et al. (2012)).

In order to determine the rotational stiffness of a single crankshaft throw, two equations can be used (Feese and Hill (2002)): Carter's formula (Nestorides (1958), equation 3.14) and Ker Wilson's formula (Wilson (1956), equation 3.15):

$$K_t = \frac{G\pi}{32\left[\frac{L_j+0.8L_w}{D_j^4-d_j^4} + \frac{0.75L_c}{D_c^4-d_c^4} + \frac{1.5R}{L_w W^3}\right]} \tag{3.14}$$

$$K_t = \frac{G\pi}{32\left[\frac{L_j+0.4D_j}{D_j^4-d_j^4} + \frac{L_c+0.4D_c}{D_c^4-d_c^4} + \frac{R-0.2(D_j+D_c)}{L_w W^3}\right]} \tag{3.15}$$

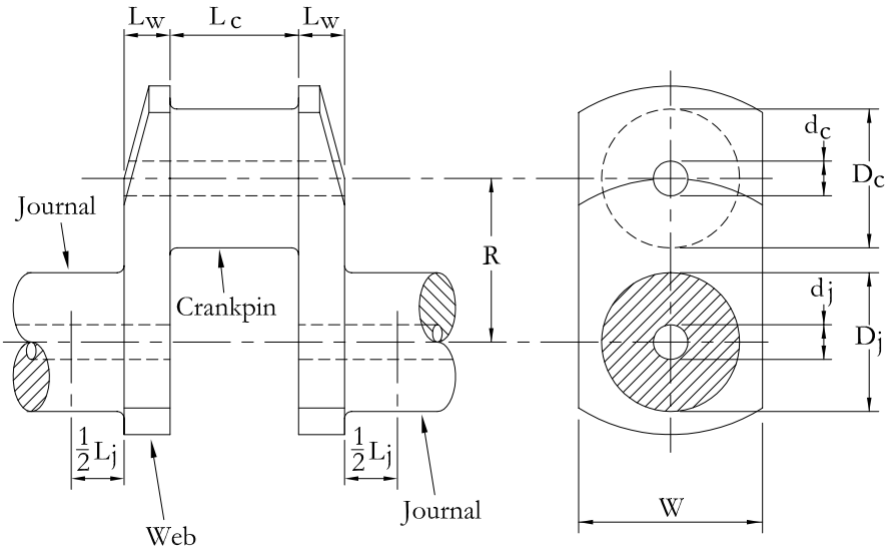

Figure 3.1: Crankshaft throw dimensions used in equations 3.14 and 3.15 – Retrieved from Feese and Hill (2002)

According to Feese and Hill (2002),

"Carter's formula is applicable to crankshafts with flexible webs and stiff journals and crankpins, while Ker Wilson's formula is better for stiff webs with flexible journals and crankpins."

3.4 Continuous shaft modelling

The theory presented in section 2.3 can be applied to a torsional vibration system. If a shaft is considered, the governing equation for a free vibration will resemble the wave equation, described by equation 3.16 (Tiwari (2010)):

$$\rho J \theta_{tt} = G J \theta_{zz} \tag{3.16}$$

where ρ is the mass density of the material, θ is the angle of rotation about the z-axis, J is the polar second moment of area and G is the shear modulus. Subscripts tt and zz denote that the second partial derivative with respect to t or z should be taken.

Note that equation 3.16 is analogous to equation 2.1, only that the area A is substituted by J, and the Young's modulus E is substituted by G.

Equation 3.16 can be solved using separation of variables and applying appropriate boundary conditions. The solution, $\theta(z,t)$ will consist of two separate functions: one depending on z, and one depending on the time, t, as shown in equation 3.17:

$$\theta(z,t) = Y(z)\ \eta(t) \tag{3.17}$$

where $Y(z)$ are the mode shapes, and $\eta(t)$ is a time-dependent function containing the natural frequency of the torsional vibration system.

The form of the solutions of $Y(z)$, i.e. the mode shapes, will depend on the types of boundary conditions applied. If a cylindrical bar of length L is considered, the three most common boundary conditions are:

1. Fixed-free – $\theta(0,t) = 0$, $\theta_z(L,t) = 0$
2. Fixed-fixed – $\theta(0,t) = \theta(L,t) = 0$
3. Free-free – $\theta_z(0,t) = \theta_z(L,t) = 0$

Put into words: The end of a bar subjected to a fixed boundary condition will not have any deflection, and the end of a bar subjected to a free boundary condition will have zero deflection growth.

The equations for natural frequencies and mode shapes for fixed-free, fixed-fixed and free-free boundary conditions are presented in table 3.1.

Table 3.1: Mode shapes and natural frequencies – Retrieved from Tiwari (2010)

S.N.	Boundary conditions	Natural frequency (rad/s)	Mode shape
1	Fixed-free	$\frac{n\pi}{2L}\sqrt{\frac{G}{\rho}}, \quad n = 1, 3, 5, \ldots$	$\sin\left(\frac{n\pi}{2L}z\right)$
2	Fixed-fixed	$\frac{n\pi}{L}\sqrt{\frac{G}{\rho}}, \quad n = 1, 2, 3, \ldots$	$\sin\left(\frac{n\pi}{L}z\right)$
3	Free-free	$\frac{n\pi}{L}\sqrt{\frac{G}{\rho}}, \quad n = 0, 1, 2, \ldots$	$\cos\left(\frac{n\pi}{L}z\right)$

In general, the mode shapes of a torsional vibration system can be assumed to be of the form (assuming the length of the system runs along the z-axis) (Tiwari (2010)):

$$Y_n(z) = A_n \cos(\alpha_n z) + B_n \sin(\alpha_n z) \tag{3.18}$$

This will later be used in conjunction with numerical results to retrieve the mode shapes of the crankshaft.

3.5 Bond graph modelling

The bond graph system representation was invented by Henry Paynter. It is a graphical approach to modelling physical systems, where the bonds represent an exchange of energy in both directions. It is well suited for modelling systems from several disciplines, including mechanical systems, electric systems and hydraulic systems. Bond graphs are also used to model the interaction between systems from these different disciplines. One example is a hydraulic system actuating a piston, which in turn applies a force to an oscillating mass-spring-damper system. One of the advantages of using bond graphs in modelling is that the same symbols are used for modelling all the different disciplines. It can also be implemented in computer software to run simulations of the system.

3.5.1 IC-field modelling

In Pedersen and Engja (2010), a procedure is suggested for developing a system of $2N$ first order differential equations, where N is the number of

generalized coordinates. This is accomplished by using the Hamilton method.

First, the generalized coordinates are defined as $\mathbf{q} = [q_1, q_2, \ldots, q_N]^T$. The generalized momentums are defined as $\mathbf{p} = [p_1, p_2, \ldots, p_N]^T$, where $p_j = \partial T/\partial \dot{q}_j$, $j = 1, 2, \ldots, N$. This is combined with the Lagrangian form of the equations of motion, yielding

$$\dot{p}_j = e'_j + Q_j, \qquad j = 1, 2, \ldots, N \tag{3.19}$$

where $e'_j = \frac{\partial T}{\partial q_j} - \frac{\partial V}{\partial q_j}$ and Q_j is the generalized force. Equation 3.19 can be written in vector form:

$$\boldsymbol{\dot{p}} = \boldsymbol{e'}(\boldsymbol{\dot{q}}, \boldsymbol{q}, t) + \boldsymbol{Q} \tag{3.20}$$

Next, the generalized momentum vector is written in matrix form as

$$\boldsymbol{p} = \boldsymbol{M}(\boldsymbol{q}, t)\boldsymbol{\dot{q}} + \boldsymbol{a}(\boldsymbol{q}, t) \tag{3.21}$$

where $\boldsymbol{M}$ is a symmetric $N \times N$ mass matrix. The vector $\boldsymbol{a}$ is only included if time-varying velocity sources are in the system. Equation 3.21 is solved to obtain the time derivative of the generalized displacements:

$$\boldsymbol{\dot{q}} = \boldsymbol{M^{-1}}(\boldsymbol{q}, t)(\boldsymbol{p} - \boldsymbol{a}) \tag{3.22}$$

Equations 3.21 and 3.22 are subsequently implemented in an IC-field in a bond graph as shown in figure 3.2.

p and **q** are then obtained by integration of efforts and flows and knowledge of initial conditions.

Next, the constitutive law for the IC-field is applied. Two systems of equations, equations 3.23 and 3.24, are obtained (Pedersen and Engja (2010)):

$$\begin{array}{rcl} p1I.f & = & \dot{q}_1 \\ p2I.f & = & \dot{q}_2 \\ \vdots & & \vdots \\ pNI.f & = & \dot{q}_N \end{array} \tag{3.23}$$

and

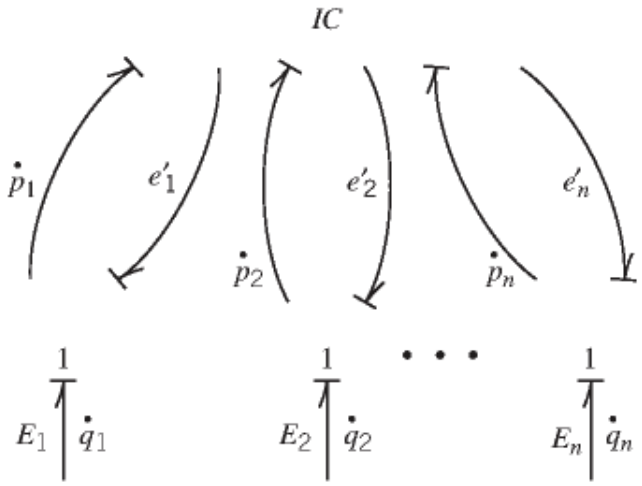

Figure 3.2: Bond graph representation of an IC-field – Retrieved from Karnopp et al. (2012)

$$\begin{array}{rcl} p1C.e & = & e'_1 \\ p2C.e & = & e'_2 \\ \vdots & & \vdots \\ pNC.e & = & e'_N \end{array} \tag{3.24}$$

where $\dot{q}_j$ is as in equation 3.22.

CHAPTER 4

Methodology

The objective of the assignment is to retrieve mathematical expressions of the torsional mode shapes of a crankshaft. This will be done by performing a frequency analysis on a finite element model (FEM) of the crankshaft.

The frequency analysis will produce a series of natural frequencies and their corresponding mode shapes. The numerically calculated displacements, $U(z)$, of each mode can then be extracted at selected locations along the crankshaft. Knowing the numerical displacement values and their corresponding location, a mathematical mode shape function, $Y(z)$, can be obtained.

The acquired mode shape functions will be used as inputs to a finite-mode bond graph model of the crankshaft. The development procedure of this type of bond graph model was covered in section 2.3.

A visualization of the methodology is shown in figure 4.1.

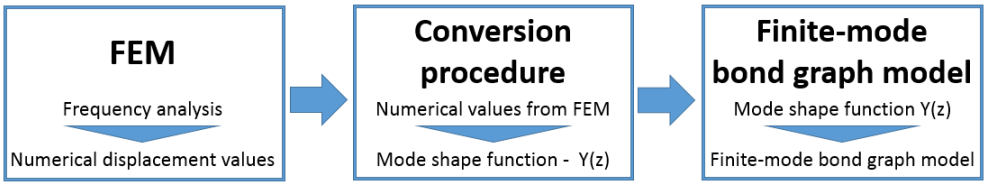

Figure 4.1: Methodology used in thesis

4.1 Finite element analysis

4.1.1 Frequency analysis

As will be explained in chapter 5, two finite element models were made: A simple shaft to verify the methodology, and a single crank throw based on a more complex finite element model.

For the simple shaft, two mesh sizes were used in order to compare results: 0.1 and 0.05.

The following boundary conditions were applied to the shaft for the frequency analysis:

1. Entire cross-sectional area at each end
   (a) No axial translation (translation along the z axis)
   (b) No rotation about the x axis
   (c) No rotation about the y axis
2. Entire outer surface along the length of the shaft:
   (a) No axial translation
   (b) No rotation about the x axis
   (c) No rotation about the y axis

The boundary conditions for the frequency analysis of the single crank were:

1. Entire cross-sectional area of each main journal
   (a) No axial translation
   (b) No rotation about the x axis
   (c) No rotation about the y axis
2. Entire outer surface of crankpin
   (a) No axial translation
   (b) No rotation about the x axis
   (c) No rotation about the y axis
3. Entire cross-sectional area of each side of each crankweb
   (a) No axial translation
   (b) No rotation about the x axis
   (c) No rotation about the y axis

These boundary conditions were used in an attempt to isolate the torsional modes.

Next, the desired outputs of the frequency analysis were defined. In this work, the Lanczos solver method was used. 30 modes were requested for the simple shaft and 20 modes for the single crank. The rigid body mode was excluded by setting the minimum frequency to 1 Hz.

After the frequency analysis was completed, displacement values for various nodes along the axial direction were picked. These values were then exported to a text file, which in turn was imported into a spreadsheet.

4.1.2 Retrieval of inertia and stiffness

The stiffness and inertia parameters of the finite element models were also retrieved. These were compared to analytical values to check whether the models were made correctly.

4.2 Conversion of numerical values to mathematical expressions

Once the numerical displacement values were obtained, they were used to generate a mathematical mode shape expression. Three z values (z_1, z_2 and z_3) and their corresponding displacement values (U_1, U_2 and U_3) were selected. A system of three equations with three unknowns could then be set up for mode n:

$$\begin{aligned} A_n \cos(\alpha_n z_1) + B_n \sin(\alpha_n z_1) &= U_1 \\ A_n \cos(\alpha_n z_2) + B_n \sin(\alpha_n z_2) &= U_2 \\ A_n \cos(\alpha_n z_3) + \underbrace{\left(\frac{U_2 - A_n \cos(\alpha_n z_2)}{\sin(\alpha_n z_2)} \right)}_{B_n} \sin(\alpha_n z_3) &= U_3 \end{aligned} \tag{4.1}$$

z_1 was always set to zero. This ensured that $A_n = U_1$ as the sine term becomes zero.

The final equation in equation set 4.1 was solved for α_n using Newton's method. A qualified initial guess was made based on the plot of the numerical data. If an unsuitable value of α_n (e.g. a negative value) was obtained, another set of z values and corresponding displacements were used. When a suitable α_n was obtained, an expression for the mode shape could be written on the form of equation 3.18.

4.3 Finite-mode bond graph model

A finite mode bond graph model of the crankshaft was created based on the approach presented in section 2.3. The obtained mode shape expressions ($Y_n(z)$) were to be used as inputs to the different elements in this bond graph model. The crank mechanism was modelled using the Lagrange-Hamiltonian approach described in section 3.5.1.

CHAPTER 5

Model Development

In this section the development of the finite element models and bond graphs of the crankshaft is described.

5.1 Finite element models

An input file for a finite element model of the crankshaft was provided by Rolls-Royce. The input file was compatible with the finite element software Abaqus.

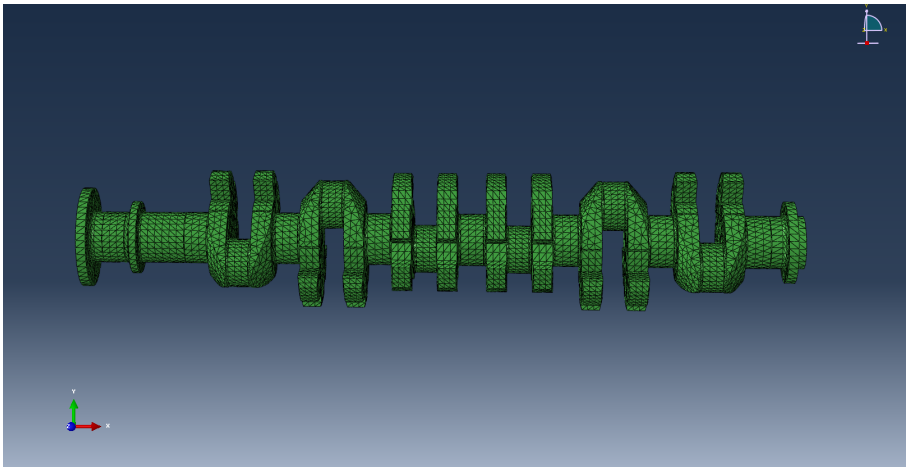

Figure 5.1: Finite element model of the crankshaft as shown in Abaqus

The finite element model of the crankshaft is shown in figure 5.1. It comes from a 6-cylinder in-line Rolls-Royce "C range" diesel engine (E. Pedersen, personal communication, October 26th, 2015). This type of engine can be found in a wide range of ships, from fishing vessels to naval vessels. The power output ranges from about 230-330 kW per cylinder (Rolls-Royce (2012)).

The material properties of the crankshaft are listed in table 5.1.

An attempt was made to run analyses on the provided crankshaft model. However, applying boundary conditions, constraints and loads was not straightfoward. There was also the matter of lack of experience with the finite element method and finite element software, so a simpler model was made based on online tutorials.

Table 5.1: Crankshaft material data retrieved from Abaqus model provided by Rolls-Royce

Description	**Value**	**Unit**
Mass density	7850	kg/m^3
Young's modulus	207	GPa
Poisson's ratio	0.3	–

5.1.1 Simple test case – 10 m long shaft

In order to get familiar with the Abaqus software, a 10 meter long shaft was made. The idea was to first work on a simple model to learn the program, then apply the lessons on the more complex model of the crankshaft. The shaft radius was set to 0.1 m. The material data were selected as shown in table 5.2:

Table 5.2: Material data – 10 m long shaft

Description	**Value**	**Unit**
Density, ρ	7850	kg/m^3
Young's modulus, E	200	GPa
Poisson's ratio, ν	0.3	–

The mesh seeds and mesh controls were set as shown in figure 5.2. Originally, a mesh size of 0.1 m was used. This was later changed to 0.05 m to gain an idea of the impact of mesh size on the accuracy of the results. For this model, a mesh size of x m means that each element measures x units in the axial direction (in this case the z-direction) of the shaft.

A zoomed in image showing the details of the resulting finite element model of the shaft is shown in figure 5.3.

In order to verify that the model was built correctly, the numerical values provided by Abaqus were compared to analytical results done by hand calculations. Specifically, the moment of inertia, I_{zz}, and the torsional stiffness, k, were checked. A comparison of analytical calculations and results that were retrieved from Abaqus can be found in section 6.1.1.

Determining the stiffness was done by fixing the shaft in one end and keeping it free in the other end. A constant torque of 100 kNm was then applied at the free end, and a job was run. The stiffness was calculated for two mesh sizes: 0.1 m and 0.05 m.

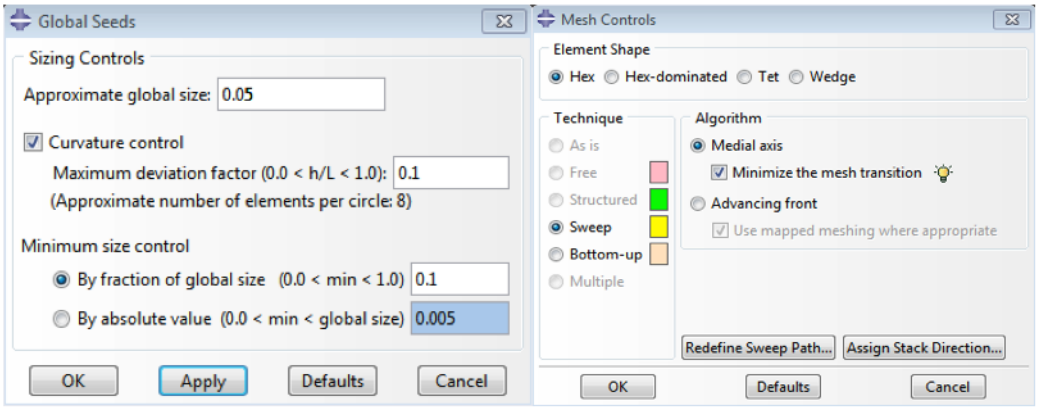

Figure 5.2: Mesh seeds and mesh controls for the simple shaft

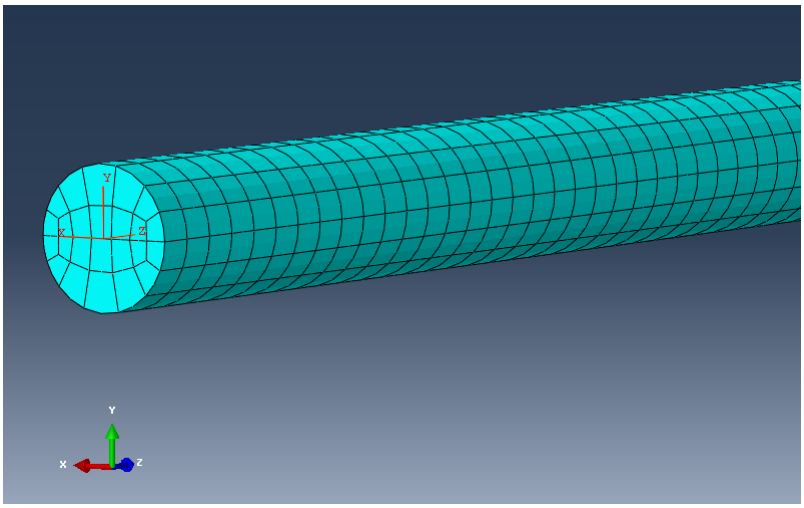

Figure 5.3: Finite element model of the simple shaft created in Abaqus

Next, a frequency analysis was carried out and the results were compared to analytical calculations. The analytical results were obtained by solving the differential equation for unforced torsional vibration, shown in equation 3.16. The free-free boundary condition was chosen. It was difficult to isolate the torsional modes in Abaqus, so lateral (and sometimes axial) modes would normally be included in the results. However, this did not appear to have any impact on the torsional modes. The frequency analysis yielded natural frequencies and corresponding mode shapes. The results of the frequency analysis can be found in section 6.1.2.

5.1.2 Single crank throw

After getting familiar with Abaqus using the simple shaft, a single crank throw based on measurements from the model in figure 5.1 was made. The reasoning behind making only a single crank throw was that it would be easier to work on, and that all the analyses would finish quicker than for a whole crankshaft.

The single crank model shown in figure 5.4 consists of two crank webs connected by a crank pin, with a half length of main journal on each crank web. The main journals, crank pin and crank webs were made as separate parts, then merged together into a single part. The material data for the single crank is the same as for the simple shaft shown in table 5.2.

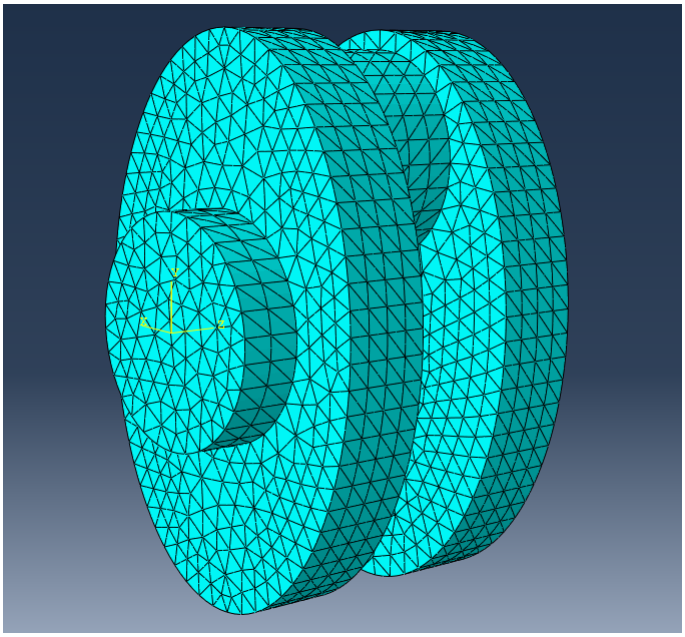

Figure 5.4: Abaqus model of a single crank

The main journals and the crank pin have a solid circular cross section, while the crank webs have a solid elliptical cross section. The dimensions of the single crank made in Abaqus are shown in figure 5.5. The dimensions of the crank webs are shown in figure 5.6.

A tetrahedral mesh of size 30 was used. The mesh seeds and mesh control dialogue boxes are shown in figure 5.7.

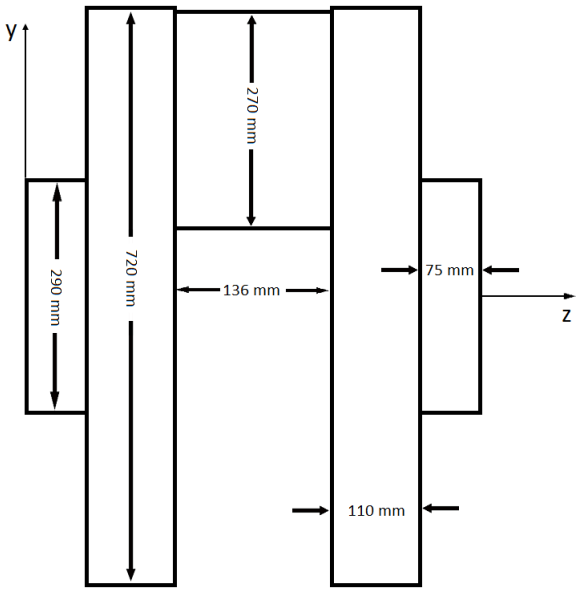

Figure 5.5: Dimensions of the single crank made in Abaqus

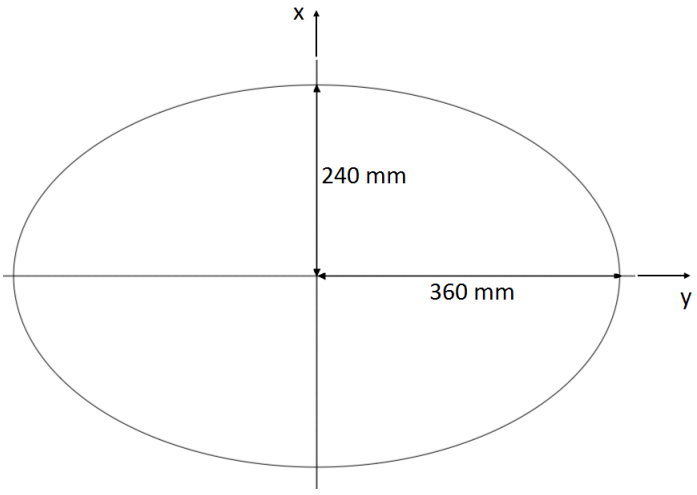

Figure 5.6: Dimensions of the crank webs

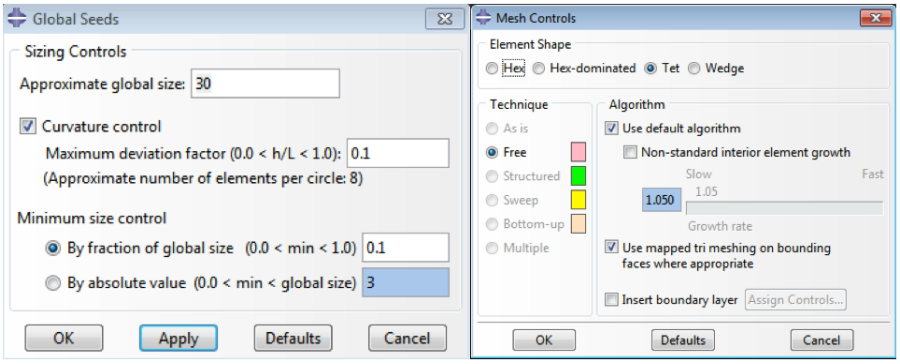

Figure 5.7: Mesh seeds and mesh controls for the single crank

5.2 Bond graphs

5.2.1 Finite-mode bond graph modelling of crank throw

The approach presented in section 2.3 was used on a single crank throw. The torque inputs were placed at $z = 0$ and $z = L$ (i.e. at the end of each main journal), as shown in figure 5.8.

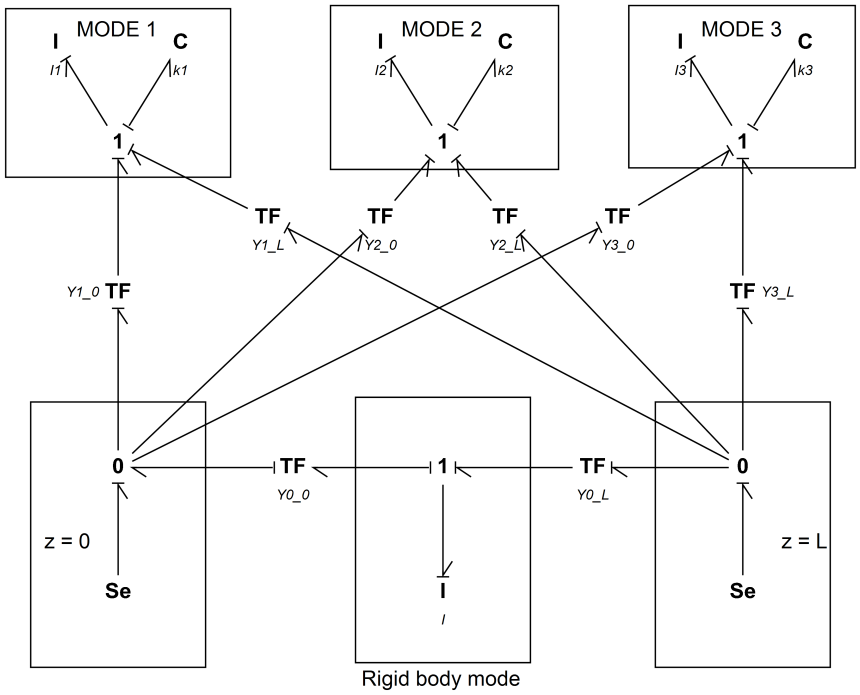

Figure 5.8: Modal bond graph representation of a single crank

Instead of modal mass m_m (equation 2.6), modal inertia was used. It is given as:

$$I_m = \int_0^L \rho A r^2 Y_m(z)^2 \, dz \tag{5.1}$$

which also means that the mth modal stiffness is:

$$k_m = I_m \omega_m^2 \tag{5.2}$$

Equation 5.1 can be rewritten to:

$$I_m = \int_0^L \frac{2I_{zz}}{L} Y_m(z)^2 \, dz \tag{5.3}$$

where I_{zz} is the moment of inertia about the z-axis and $Y_m(z)$ is the mth mode shape expression retrieved from the finite element model. For the main journals, which have a cylindrical cross section, the modal inertia is as written in equation 5.1. For the crank pin, the contribution from the parallel axis theorem (equation 3.11) must be included in the I_{zz} term in equation 5.3. For the crank webs, which have an elliptical cross section with moment of inertia as given in equation 3.10, the modal inertia is:

$$I_{m,CW} = \int_0^{L_{CW}} \frac{2I_{zz,CW}}{L_{CW}} Y_m(z)^2 \, dz = \int_0^{L_{CW}} \frac{\rho\pi ab}{2}(a^2+b^2) Y_m(z)^2 \, dz \tag{5.4}$$

The mth modal inertia of a single crank thus becomes:

$$\begin{aligned} I_m = &\int_0^{75\ mm} \frac{2I_{zz,MJ}}{L_{MJ}} Y_m(z)^2 \, dz \\ &+ \int_{75\ mm}^{185\ mm} \frac{2I_{zz,CW}}{L_{CW}} Y_m(z)^2 \, dz \\ &+ \int_{185\ mm}^{321\ mm} \frac{2I_{zz,CP}}{L_{CP}} Y_m(z)^2 \, dz \\ &+ \int_{321\ mm}^{431\ mm} \frac{2I_{zz,CW}}{L_{CW}} Y_m(z)^2 \, dz \\ &+ \int_{431\ mm}^{506\ mm} \frac{2I_{zz,MJ}}{L_{MJ}} Y_m(z)^2 \, dz \end{aligned} \tag{5.5}$$

where the subscripts MJ, CW and CP stand for main journal, crank web and crank pin respectively. The integration limits are in accordance with the measurements shown in figure 5.5.

5.2.2 IC-field representation of a single crank

Based on the models and equations derived in section 2.3 and the theory presented in section 3.5.1, an IC-field representation of the single crank could

be made. Comparing equation 3.19 and 2.5, it is evident that the term $-k_m q_m$ in the latter will replace the term e'_j in the former. Further, $p_m = I_m \dot{q}_m \Leftrightarrow \dot{q}_m = p_m / I_m$. The constitutive laws for the IC field of the crankshaft can thus be written:

$$\begin{aligned} pmI.f &= \dot{q}_m = \frac{p_m}{I_m} \\ pmC.e &= \dot{p}_m = -k_m q_m \end{aligned} \tag{5.6}$$

where m is the mode number.

5.2.3 Crank mechanism modelling

A sketch of the crank mechanism is shown in figure 5.9.

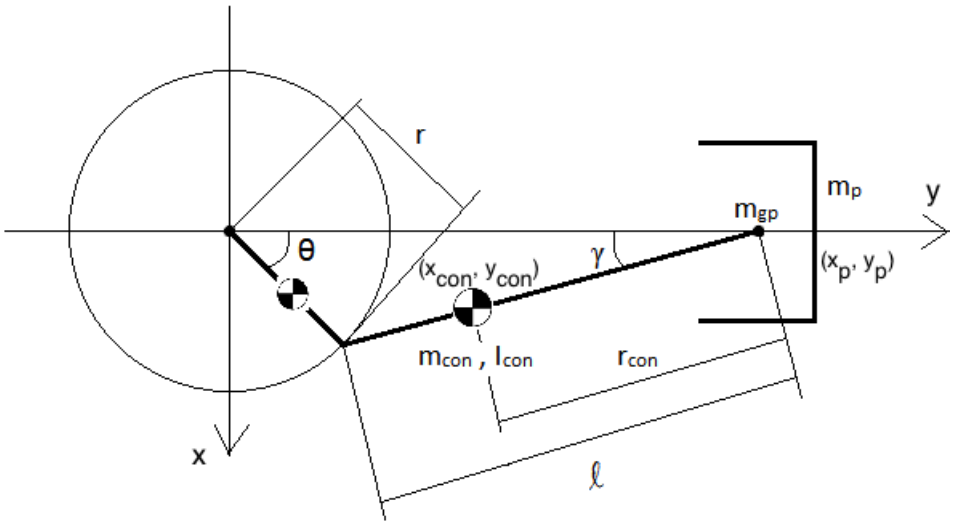

Figure 5.9: Sketch of crank mechanism

- θ is the crank angle
- γ is the angle the connecting rod makes with the y-axis
- m_p, m_{gp} and m_{con} are the masses of the piston, gudgeon pin and connecting rod respectively

- I_{con} is the mass moment of inertia of the connecting rod
- (x_{con}, y_{con}) are the coordinates of the connecting rod's center of mass
- (x_p, y_p) are the coordinates of the piston's and gudgeon pin's center of mass
- r is the crank radius
- r_{con} is the distance from the gudgeon pin to the connecting rod's center of mass
- l is the length of the connecting rod

Additionally, the geometric relations in equation 5.7 apply:

$$\begin{aligned}
\lambda &= \frac{r}{l} \\
x_{con} &= r\sin\theta \\
y_{con} &= r\cos\theta + (l - r_{con})\sqrt{1-(\lambda\sin\theta)^2} \\
y_p &= r(\cos\theta + \frac{1}{\lambda}\sqrt{1-(\lambda\sin\theta)^2} \\
\dot{x}_{con} &= r_{con}\lambda\dot{\theta}\cos\theta \\
\dot{y}_{con} &= -r\sin\theta - (l - r_{con})\frac{\lambda^2\sin\theta\cos\theta}{\sqrt{1-(\lambda\sin\theta)^2}}\dot{\theta} \\
\dot{y_p} &= -r\left(\sin\theta + \frac{\lambda\sin\theta\cos\theta}{\sqrt{1-(\lambda\sin\theta)^2}}\right)\dot{\theta} \\
\cos\gamma &= \sqrt{1-(\lambda\sin\theta)^2}
\end{aligned}$$

The mass and the moment of inertia of the crank throw are omitted in the following calculations, as they are included in the modal IC-field representation of the crankshaft.

The kinetic energy T and potential energy V of the crank mechanism can be expressed as (Polić et al. (2016)):

$$T = \frac{1}{2}\Big((I_{con} + m_{con}r_{con}^2)\dot{\gamma}^2 + m_{con}(\dot{x}_{con}^2 + \dot{y}_{con}^2) + (m_{gp} + m_p)\dot{y}_p^2\Big) \tag{5.7}$$

$$V = m_{con}gy_{con} + (m_p + m_{gp})gy_p + F_{cyl}y_3 \tag{5.8}$$

where g is the gravitational acceleration and F_{cyl} is the combustion gas force working on the piston.

The momentum $p = \partial T/\partial\dot{\theta}$ of the crank mechanism is:

$$\frac{\partial T}{\partial \dot{\theta}} = I_{CM}\dot{\theta} \tag{5.9}$$

where I_{CM} is the inertia of the crank mechanism:

$$\begin{aligned} I_{CM} = {} & (I_{con} + m_{con}r_{con}^2)\frac{(\lambda\cos\theta)^2}{1-\lambda^2\sin^2\theta} + m_{con}(r_{con}\lambda\cos\theta)^2 \\ & + (m_p + m_{gp})\left(-r\left(\sin\theta + \frac{\lambda\sin\theta\cos\theta}{\sqrt{1-\lambda^2\sin^2\theta}}\right)\right)^2 \\ & + m_{con}\left(-r\sin\theta - (l-r_{con})\frac{\lambda^2\sin\theta\cos\theta}{\sqrt{1-(\lambda\sin\theta)^2}}\right)^2 \end{aligned} \tag{5.10}$$

Next, the partial derivative of the Lagrangian, $L = T - V$, with respect to the crank angle is needed:

$$\begin{aligned} \frac{\partial T}{\partial\theta} = {} & \frac{1}{2}\Bigg[(I_{con} + m_{con}r_{con}^2)\left(\frac{2\lambda^4\sin\theta\cos^3\theta}{(1-\lambda^2\sin^2\theta)^2} - \frac{2\lambda^2\sin\theta\cos\theta}{1-\lambda^2\sin^2\theta}\right) \\ & - 2m_{con}(r\lambda)^2\sin\theta\cos\theta + (m_p+m_{gp})\Bigg(2r^2\Bigg(\sin\theta \\ & + \frac{\lambda\sin\theta\cos\theta}{\sqrt{1-\lambda^2\sin^2\theta}}\Bigg)\Bigg(\cos\theta - \frac{\lambda}{\sqrt{1-\lambda^2\sin^2\theta}} + \frac{\lambda^3\sin^3\theta\cos^2\theta}{\sqrt{(1-\lambda^2\sin^2\theta)^3}}\Bigg)\Bigg) \\ & - 2m_{con}\left(\frac{\lambda^2(l-r_{con})\sin\theta\cos\theta}{\sqrt{1-(\lambda\sin\theta)^2}} + r\sin\theta\right)\Bigg(\frac{\lambda^2(l-r_{con})}{\sqrt{1-(\lambda\sin\theta)^2}} \\ & + \frac{\lambda^4(l-r_{con})(\sin\theta\cos\theta)^2}{(1-(\lambda\sin\theta)^2)^{3/2}} + r\cos\theta\Bigg)\Bigg]\dot{\theta}^2 \end{aligned} \tag{5.11}$$

$$\begin{aligned}\frac{\partial V}{\partial \theta} = m_{con}g\Bigg(&- r\sin\theta - (l - r_{con})\frac{\lambda^2 \sin\theta\cos\theta}{\sqrt{1-\lambda^2\sin^2\theta}}\Bigg) \\ &+ (m_p g + m_{gp}g + F_{cyl})r\Bigg(- \sin\theta - \frac{\lambda\sin\theta\cos\theta}{\sqrt{1-\lambda^2\sin^2\theta}}\Bigg)\end{aligned} \tag{5.12}$$

The ignition phase angle of a four-stroke engine with six cylinders is (Pedersen and Valland (2014)) $\Delta\theta = 720°/\ 6 = 120°$. The firing order is 1-5-3-6-2-4. Therefore, the ignition angle of each cylinder is as shown in table 5.3.

Table 5.3: Ignition angles

$\Delta\theta_1$	$\Delta\theta_2$	$\Delta\theta_3$	$\Delta\theta_4$	$\Delta\theta_5$	$\Delta\theta_6$
0°	480°	240°	600°	120°	360°

The ignition angle must be subtracted from the crank angle θ at the respective cylinder position in the bond graph.

With equations 5.9, 5.11, 5.12 and table 5.3, the constitutive laws for the IC-field can be written (equation 5.13).

$$\begin{aligned} pI.f = \dot{\theta} &= \frac{p}{I_{CM}} \\ pC.e = e' &= \frac{\partial T}{\partial \theta} - \frac{\partial V}{\partial \theta}\end{aligned} \tag{5.13}$$

5.2.4 Complete crankshaft bond graph model

With the modelling procedure for the single crank throw and the crank mechanism in place, a complete model of the crankshaft system can be made. The crank mechanism sub-model is simply attached to the zero junctions representing the end of each main journal. It will then act as a torque input to the single crank sub-model.

As seen in figure 5.10, two extra modal compliances (C elements) have been attached: One to each zero junction. According to Karnopp et al. (2012), one extra modal compliance can be added to the model for each external force input with flow-in causality. Normally an I element would accompany

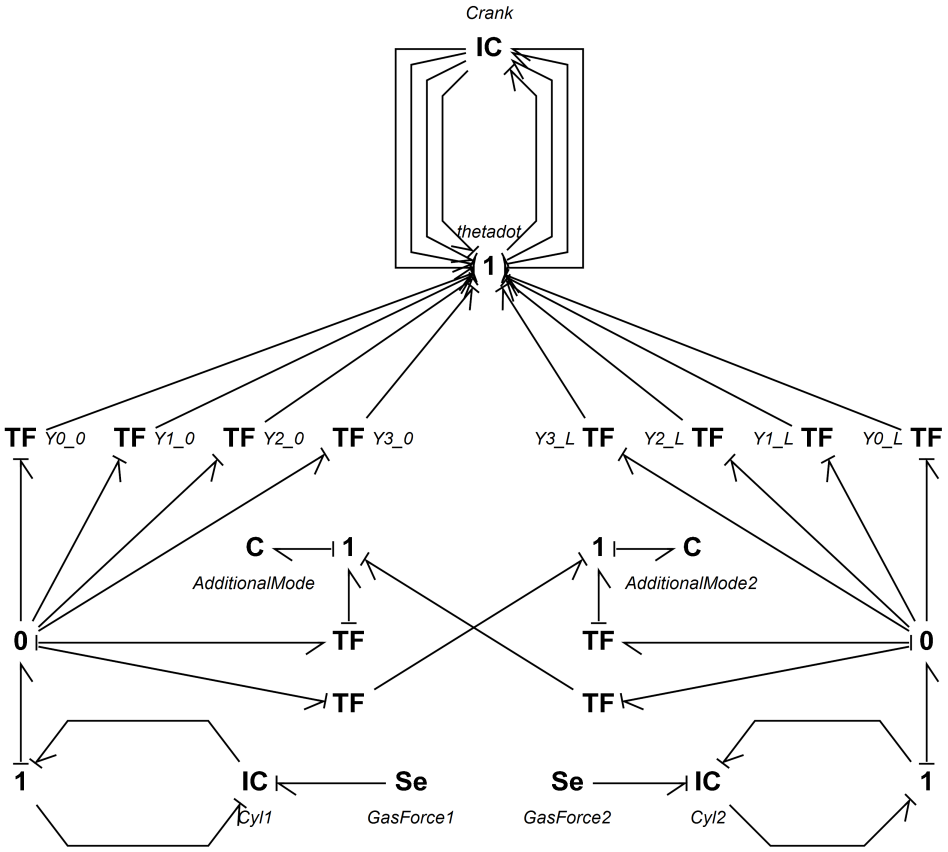

Figure 5.10: Bond graph model of the single crank and crank mechanism

the C element, but Karnopp et al. (2012) notes that the additional modes are stiffness controlled. This means that the system response will only to a negligible degree be affected by the extra modal inertia.

The bond graph in figure 5.10 can also be represented as a vector bond graph as shown in figure 5.11.

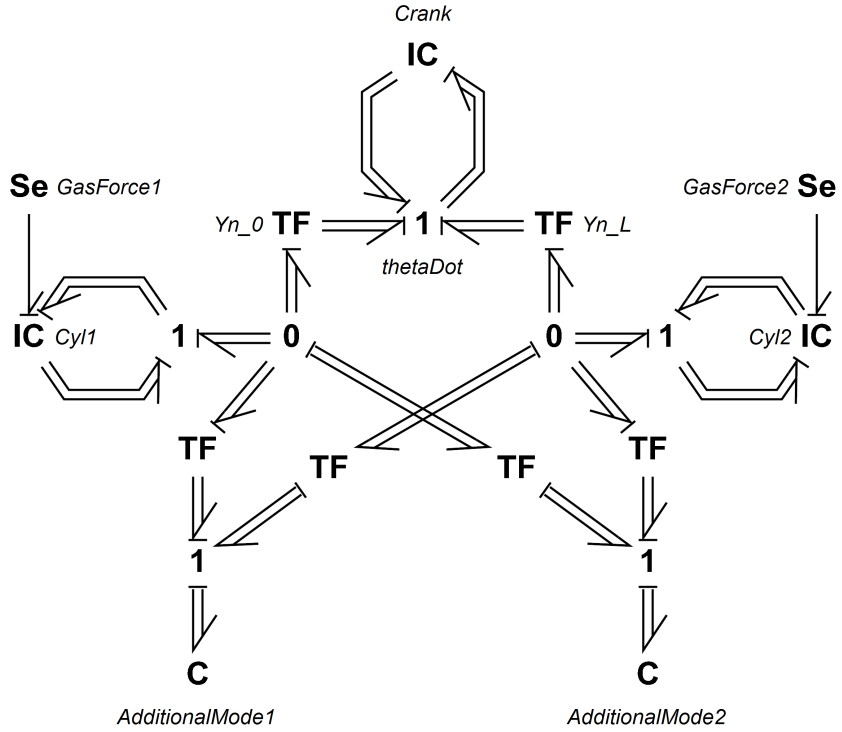

Figure 5.11: Vector bond graph model of the single crank and crank mechanism

However, the mode shapes are needed in order to input the correct transformer moduli in the TF elements and to get the correct modal inertias and modal stiffnesses. In chapter 6, the results of a frequency analysis are presented. The aim of the frequency analysis was to obtain the mode shapes of a single crank throw. If successful, the approach would be applied for the whole crankshaft.

CHAPTER 6

Results

In this chapter, the method for converting the mode shapes from numerical values provided by the finite element model to mathematical expressions is verified. The results of the analyses are also shown. The results from the analysis of the single crank are of particular interest, as they are needed as inputs to the finite-mode bond graph model.

6.1 Verification of methodology – Case study of a simple shaft

In order to verify the methodology, it was applied to a model of a simple shaft. This was done because the correct mode shapes for such a geometry are well-known, so potential shortcomings in the method should become evident.

6.1.1 Stiffness and inertia data

Stiffness and inertia parameters for the simple shaft were retrieved to check that the model was made correctly and to gain some experience with Abaqus. The analytical and numerical values for inertia and stiffness are displayed in table 6.1:

Table 6.1: Analytical and numerical values of inertia and stiffness

Property	Analytical	Numerical (Abaqus)	Error
Mass moment of inertia $[kgm^2]$	12,33	12,33	0
Torsional stiffness $[Nm/rad]$, mesh size 0.1	1,208,304	1,122,965	7.06 %
Torsional stiffness $[Nm/rad]$, mesh size 0.05	1,208,304	1,208,201	0.02 %

A closer look at the mesh on the end of the shaft experiencing torque is shown in figure 6.1. This screenshot was taken after applying the torque

with a mesh size of 0.1 m.

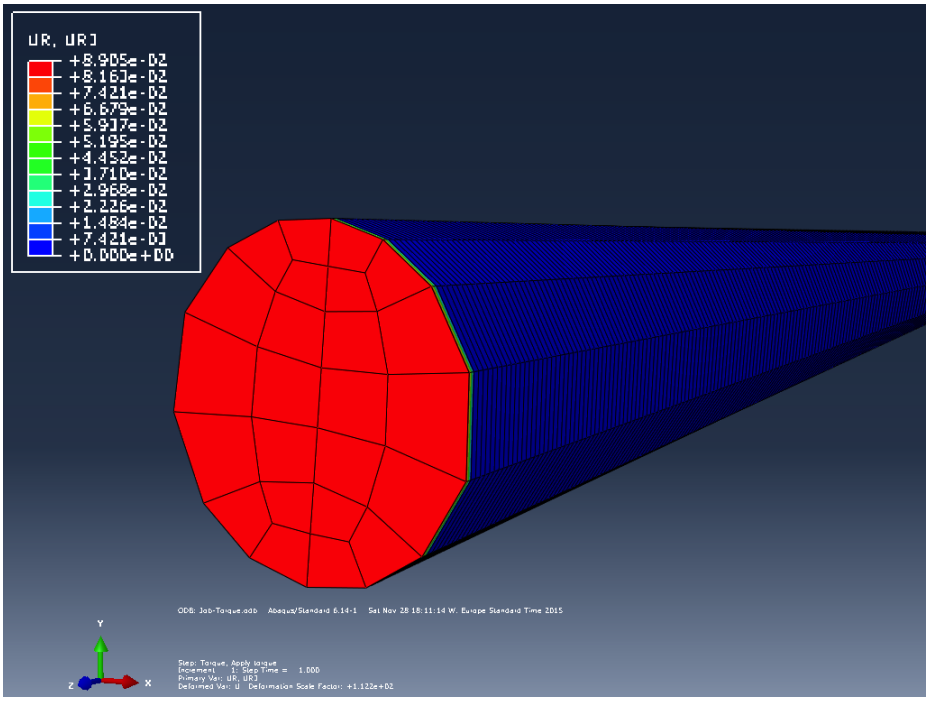

Figure 6.1: Visualization of rotational displacement at the torque-loaded end of the simple shaft. Torque: 100 kNm, mesh size 0.1 m

The moment of inertia about the z-axis of the shaft is given analytically in equation 3.9. As seen in table 6.1, the moment of inertia about the z-axis given by Abaqus matched the analytical moment of inertia exactly.

The magnitude of the rotation about the z-axis at the free end was found to be $8.278 \cdot 10^{-2}\ rad$ with a mesh size of 0.05 m. This means that the stiffness is:

$$k = \frac{100\ kNm}{8.278 \cdot 10^{-2}\ rad} = 1,208,201\ \frac{Nm}{rad}$$

The analytical stiffness was found using equation 3.12, with $G = 76.92$ GPa.

6.1.2 Frequency analysis

A comparison of the natural frequencies calculated by Abaqus and their analytical counterparts is shown in table 6.2:

Table 6.2: Natural frequencies corresponding to modes 1, 2 and 3 – Analytical vs. numerical

Mode	$f_{analytical}$ **[Hz]**	f_{Abaqus} **[Hz]**	**Error**
1	156,52	156,52	0
2	313,04	313,04	0
3	469,55	469,56	0,002 %

Visualizations of the first three non-rigid mode shapes calculated by Abaqus are shown in figures 6.2, 6.3 and 6.4. The displacements seemed to be given in absolute values, as the minimum displacement magnitude was zero for all modes.

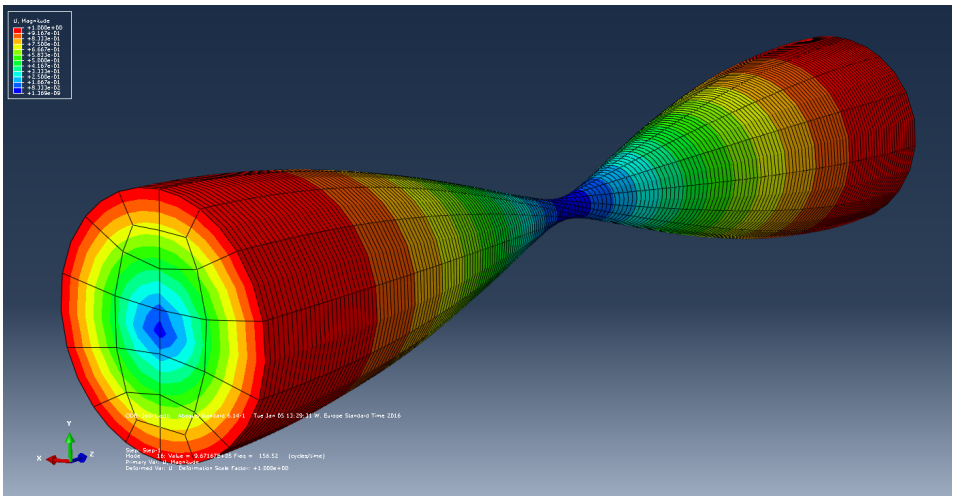

Figure 6.2: Torsional mode 1 retrieved from frequency analysis in Abaqus

Figure 6.2 shows the displacement of the first non-rigid torsional mode with free-free boundary conditions. The box in the top left corner shows the values corresponding to the different colors along the shaft. Red and blue corresponds to maximum and minimum displacement magnitude respectively. The maximum displacement magnitude is 1, while the minimum is 0.

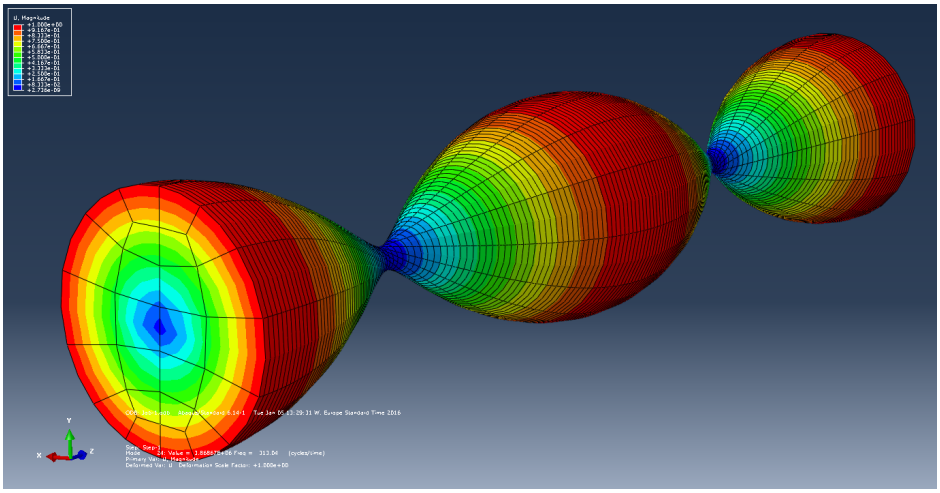

Figure 6.3: Torsional mode 2 retrieved from frequency analysis in Abaqus showing the twist of the mesh lines

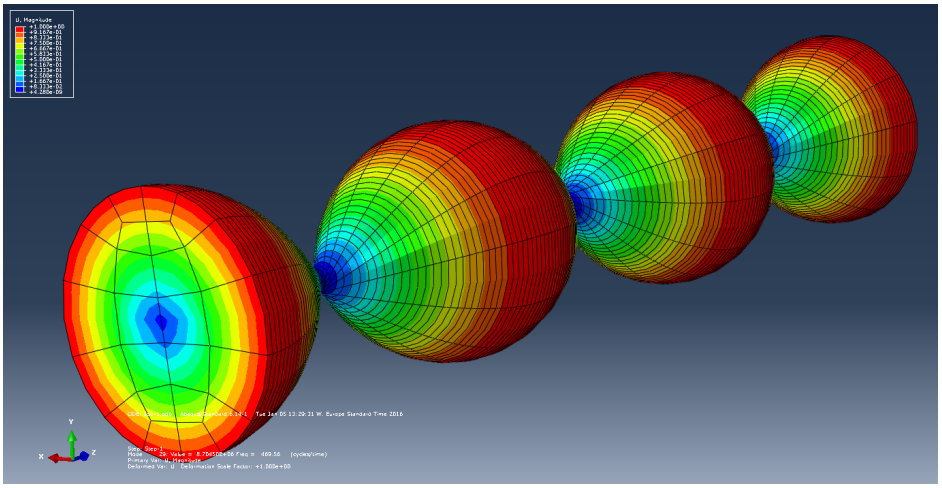

Figure 6.4: Screenshot of torsional mode 3 as shown in Abaqus

In order to obtain an expression for the mode shape of the shaft on the form of equation 3.18, displacement values for three z-positions were taken. The rest of the displacement values can be found in appendix A. The z-values and their respective displacements chosen for each mode are presented in table 6.3:

For modes 1, 2 and 3, equations 6.5, 6.6 and 6.7 respectively were set up:

Table 6.3: Selected values for retrieval of mode shape expressions (normalized)

Mode 1		**Mode 2**		**Mode 3**	
z [m]	U_1	**z [m]**	U_2	**z [m]**	U_3
0.00	1.000	0.00	1.000	0.00	1.000
3.90	0.339	1.95	0.339	1.40	0.249
7.00	-0.587	6.70	-0.482	2.90	-0.918

$$\cos(7\alpha_1) + \frac{0.339 - \cos(3.9\alpha_1)}{\sin(3.9\alpha_1)} \sin(7\alpha_1) = -0.587 \tag{6.1}$$

$$\cos(6.7\alpha_2) + \frac{0.339 - \cos(1.95\alpha_2)}{\sin(1.95\alpha_2)} \sin(6.7\alpha_2) = -0.482 \tag{6.2}$$

$$\cos(2.9\alpha_3) + \frac{0.249 - \cos(1.4\alpha_3)}{\sin(1.4\alpha_3)} \sin(2.9\alpha_3) = -0.918 \tag{6.3}$$

These equations were solved for α_n ($n = 1,\ 2,\ 3$) using Newton's method. For mode 2 and 3 the initial guess was set to 0.5, while for mode 1 it was set to 0.1. The following values were obtained:

- $B_1 = -0.343 \cdot 10^{-3}$
- $B_2 = -0.924 \cdot 10^{-3}$
- $B_3 = 0.729 \cdot 10^{-3}$
- $\alpha_1 = 0.314$
- $\alpha_2 = 0.628$
- $\alpha_3 = 0.943$

which produced the following expressions for the first three mode shapes (excluding the rigid body mode):

$$\begin{aligned} Y_1(z) &= \cos(0.314z) - 0.343 \cdot 10^{-3} \sin(0.314z) \\ Y_2(z) &= \cos(0.628z) - 0.924 \cdot 10^{-3} \sin(0.628z) \\ Y_3(z) &= \cos(0.943z) + 0.729 \cdot 10^{-3} \sin(0.943z) \end{aligned} \tag{6.4}$$

Plots of the retrieved values from Abaqus vs. the corresponding mode shape functions from equation 6.4 are shown in figures 6.14, 6.15, and 6.16. As seen in the figures, the graphs of the retrieved mode shape functions match the plots of the corresponding numerical points very well.

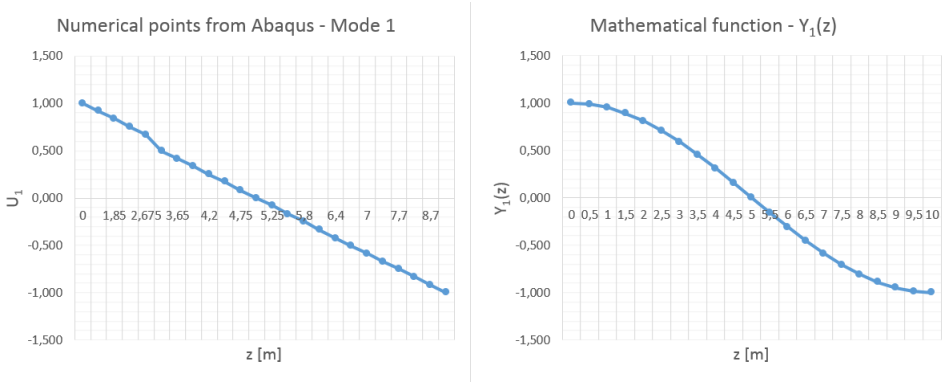

Figure 6.5: Plot of numerical values retrieved from Abaqus and the corresponding mode shape function $Y_1(z)$

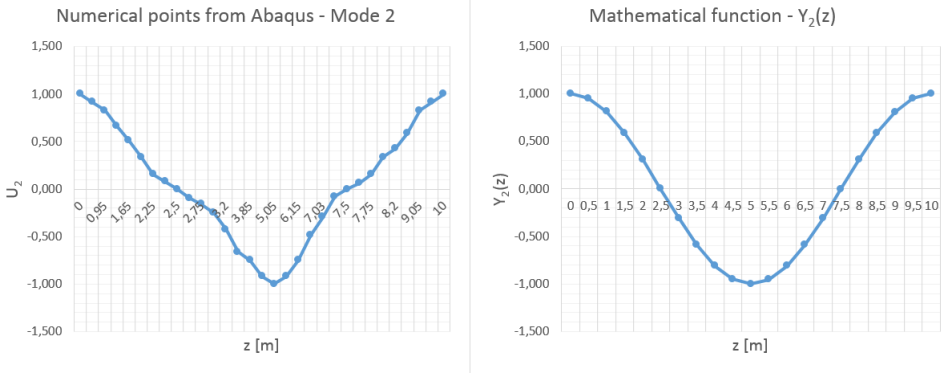

Figure 6.6: Plot of numerical values retrieved from Abaqus and the corresponding mode shape function $Y_2(z)$

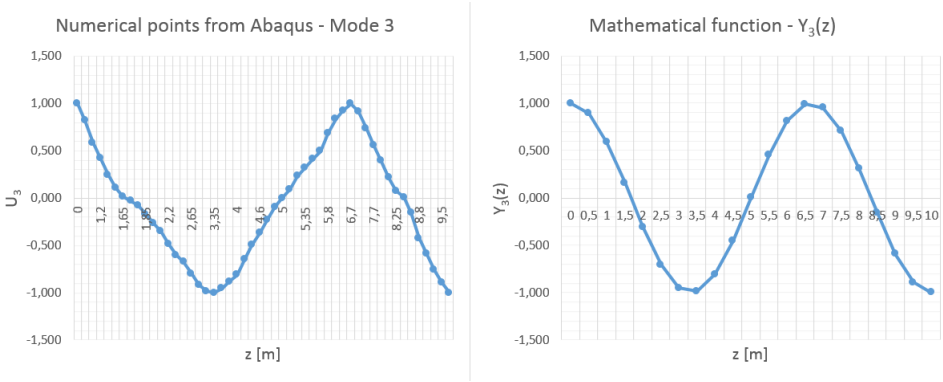

Figure 6.7: Plot of numerical values retrieved from Abaqus and the corresponding mode shape function $Y_3(z)$

For a 10 m long shaft with the free-free boundary condition, the analytical expressions for the nth natural frequency and mode shape are given in table 3.1. The first three analytical mode shapes (using $L = 10$) are plotted in figure 6.8.

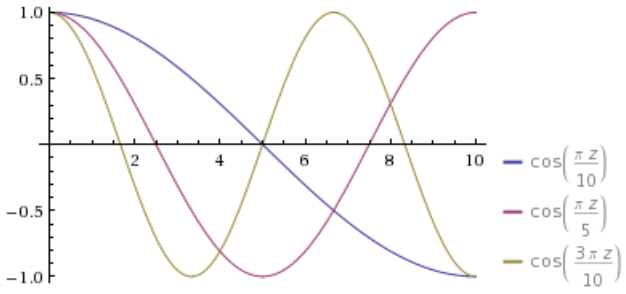

Figure 6.8: Plot of the first three non-rigid analytical mode shape functions

6.2 Analysis of a single crank throw

6.2.1 Inertia and stiffness

The mass moment of inertia about the z-axis of the single crank model was retrieved using the query tool in Abaqus. It was found to be $2.58{\cdot}10^7\ kg\ mm^2 = 25.8\ kg\ m^2$. The analytical result using equations 3.9, 3.10 and 3.11 gave the result $I_{zz} = 25,759,909\ kg\ mm^2 \approx 25.8\ kg\ m^2$.

The stiffness of the single crank throw was determined numerically by using Abaqus, and by using equations 3.14 and 3.15. To determine the stiffness in

Abaqus, a boundary condition fixing one of the main journals was applied. A constant torque of 500 kNm was applied at the center of the cross section of the main journal on the opposite side. The angular displacement due to the applied torque calculated by Abaqus is shown in figure 6.9. The maximum value appears at the free end, and is UR3 = $5.747 \cdot 10^{-3}$ *rad*. The applied torque was then divided by the angular displacement at the free end to obtain the stiffness.

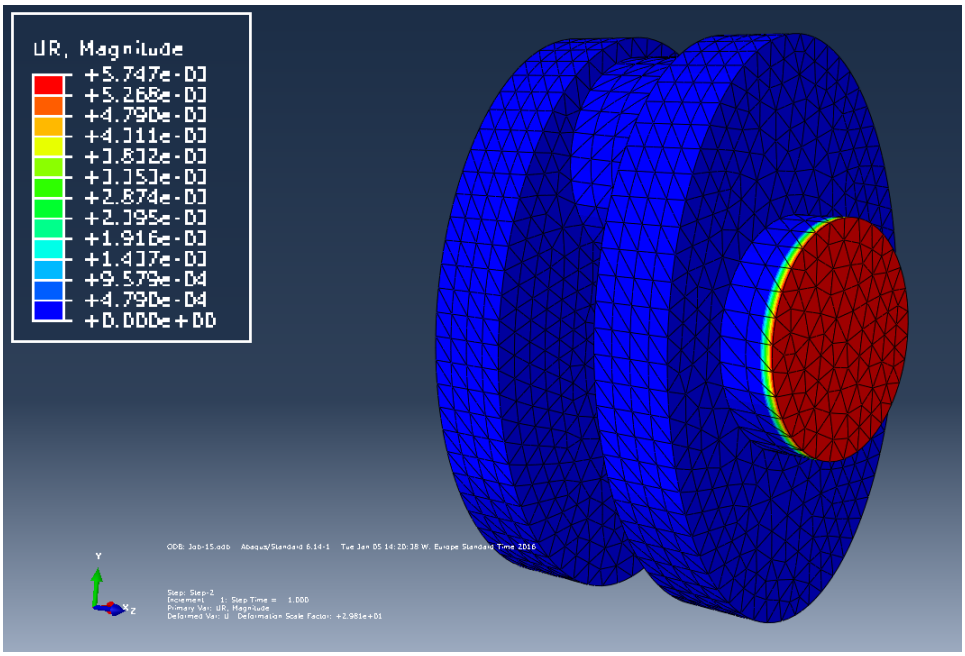

Figure 6.9: Angular displacement of the single crank shown in Abaqus

A comparison of the formula-based and numerical stiffnesses is shown in table 6.4.

Table 6.4: Stiffness data for single crank retrieved from Abaqus and formulas

Description	**Value**	**Unit**
Carter stiffness	$9.7 \cdot 10^7$	Nm/rad
Ker Wilson stiffness	$8.3 \cdot 10^7$	Nm/rad
Abaqus stiffness	$8.7 \cdot 10^7$	Nm/rad

6.2.2 Frequency analysis – Case 1

The mode shape functions of the single crank were needed. To obtain them, a frequency analysis was done on the finite element model in Abaqus.

The resultant vector view of mode 1, 2 and 3 are shown in figures 6.10, 6.11 and 6.12. This view of the modes was useful, as it made it possible to determine the sign of the displacement values based on the direction of the arrows. Their sign was manually inserted when they were entered in a spreadsheet. In the legend in the top left corner of each figure, the red colour represents a 1 mm displacement, while the blue colour represents 0 mm displacement.

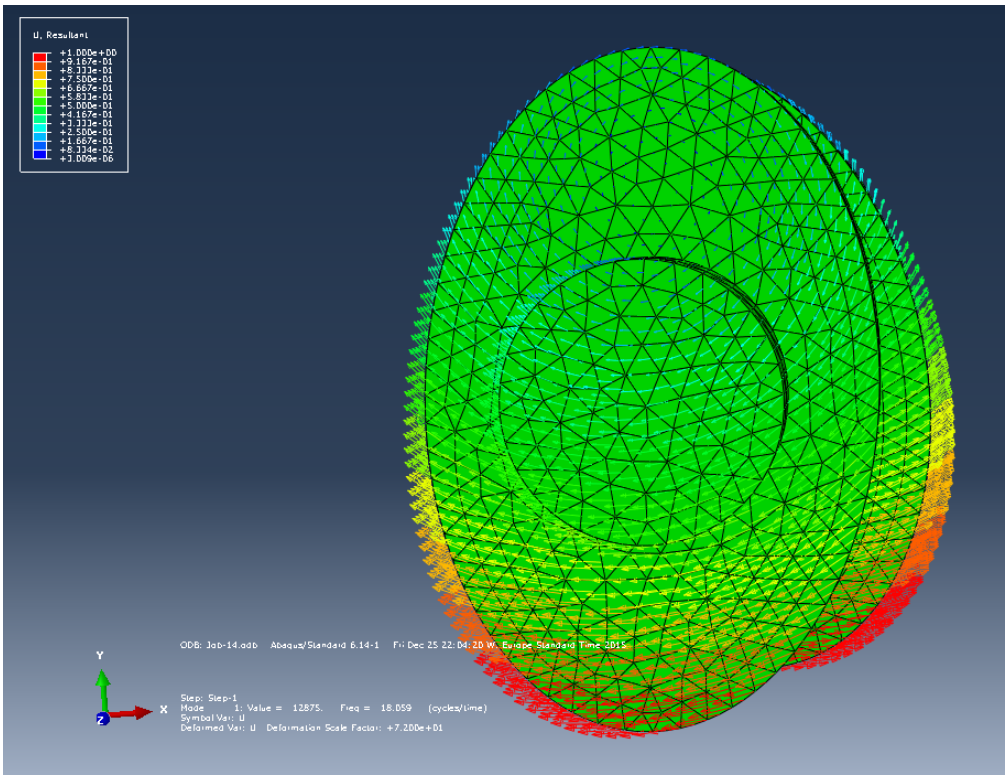

Figure 6.10: Resultant vector view of mode 1

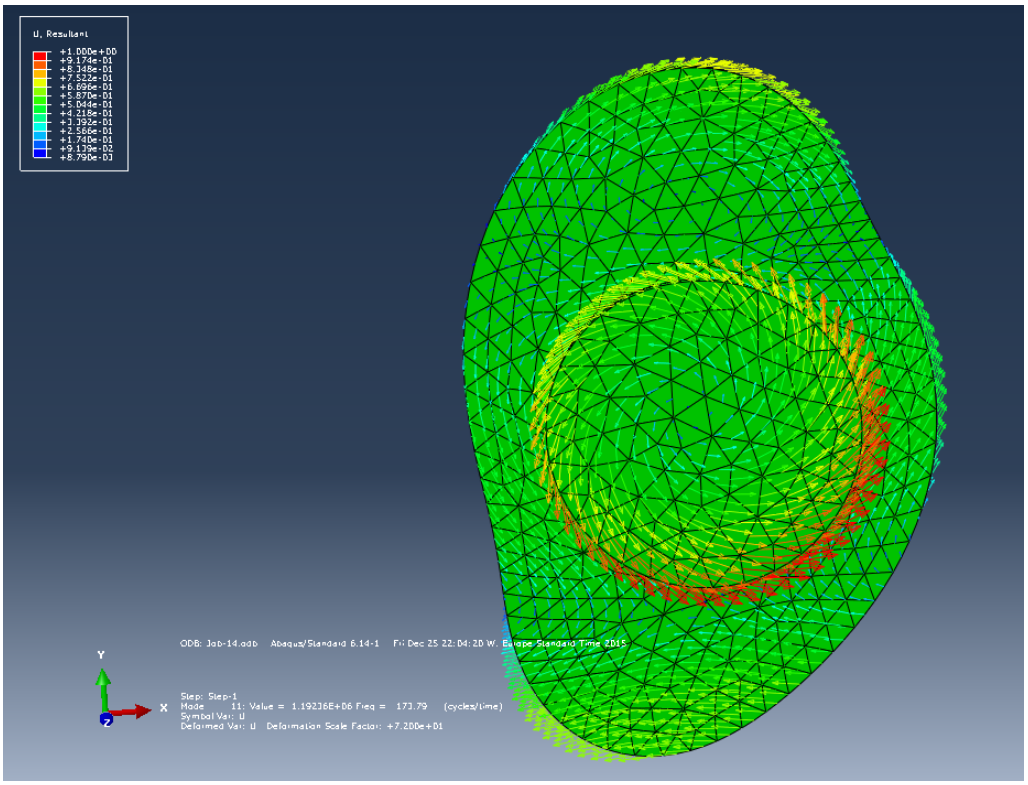

Figure 6.11: Resultant vector view of mode 2

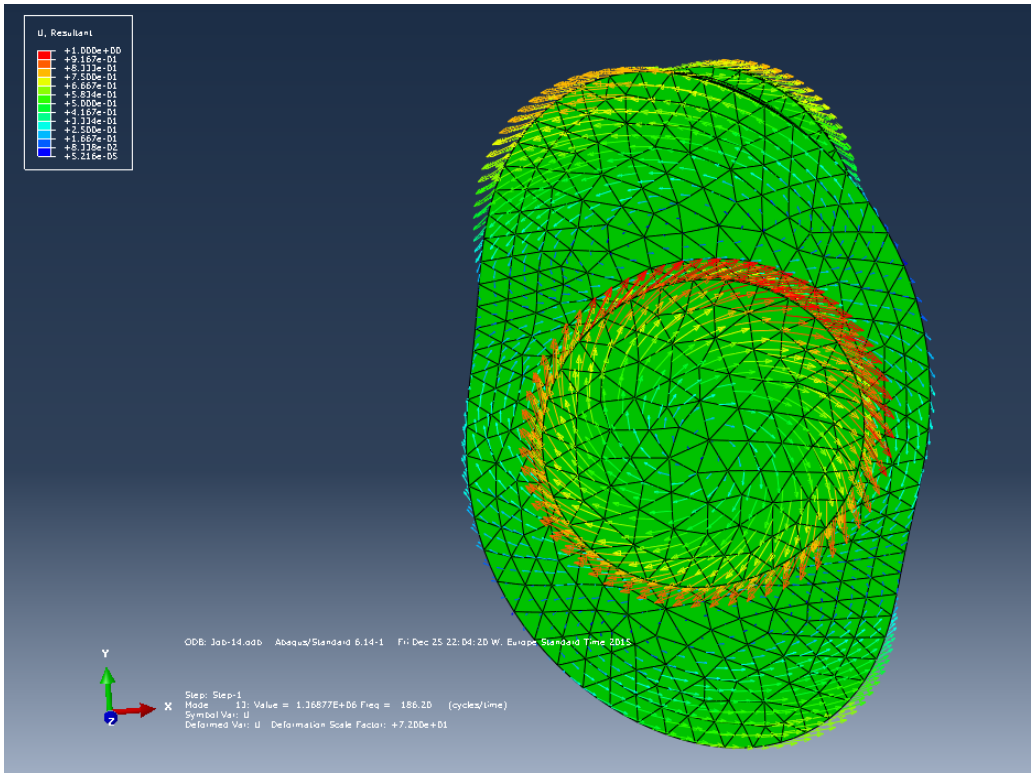

Figure 6.12: Resultant vector view of mode 3

17 displacement values were taken for different z-values along the crank length for each mode shape. The nodes at which the values were taken are shown in figure 6.13. All the displacement values can be found in appendix B.

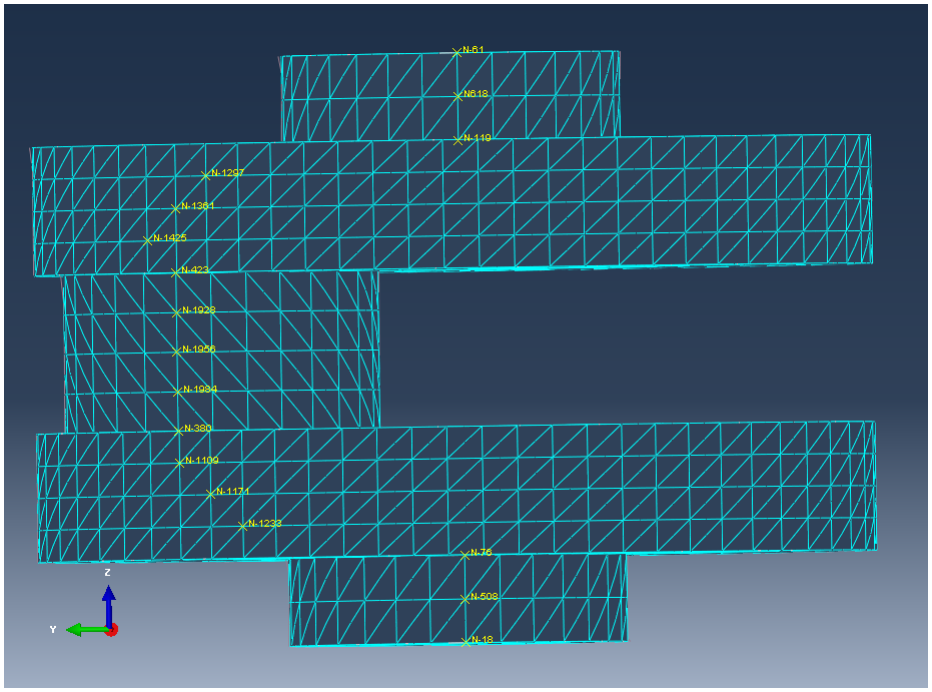

Figure 6.13: Illustration of nodes queried to retrieve mode shapes for the single crank

The same procedure as in section 6.1.2 was used. As for the simple shaft, displacement values for three z-positions were taken. The z-values and their respective displacements chosen for each mode are presented in table 6.5.

Table 6.5: Selected values for retrieval of mode shape expressions (normalized)

Mode 1		**Mode 2**		**Mode 3**	
z [mm]	U_{norm}	**z [mm]**	U_{norm}	**z [mm]**	U_{norm}
0.0	1.000	0.0	1.000	0.0	1.000
130.0	0.620	75.0	0.626	37.5	0.887
321.0	-0.277	130.0	-0.065	102.5	-0.151

Equation set 4.1 was again set up for each mode. For modes 1, 2 and 3, equations 6.5, 6.6 and 6.7 respectively were obtained:

$$\cos(321\alpha_1) + \frac{0.620 - \cos(130\alpha_1)}{\sin(130\alpha_1)} \sin(321\alpha_1) = -0.277 \tag{6.5}$$

$$\cos(130\alpha_2) + \frac{0.626 - \cos(75\alpha_2)}{\sin(75\alpha_2)} \sin(130\alpha_2) = -0.065 \tag{6.6}$$

$$\cos(102.5\alpha_3) + \frac{0.887 - \cos(37.5\alpha_3)}{\sin(37.5\alpha_3)} \sin(102.5\alpha_3) = -0.151 \tag{6.7}$$

These equations were solved for α_n ($n = 1,\ 2,\ 3$) using Newton's method, with an initial guess of 0.01 for all three equations. The following values were obtained:

- $B_1 = -0.358$
- $B_2 = 0.106$
- $B_3 = 0.321$
- $\alpha_1 = 0.0046$
- $\alpha_2 = 0.0133$
- $\alpha_3 = 0.0186$

which produced the following expressions for the first three mode shapes (excluding the rigid body mode):

$$\begin{aligned} Y_1(z) &= \cos(0.0046z) - 0.358\sin(0.0046z) \\ Y_2(z) &= \cos(0.0133z) + 0.106\sin(0.0133z) \\ Y_3(z) &= \cos(0.0186z) + 0.321\sin(0.0186z) \end{aligned} \tag{6.8}$$

Plots of the retrieved values from Abaqus vs. the corresponding mode shape functions are shown in figures 6.14, 6.15, and 6.16.

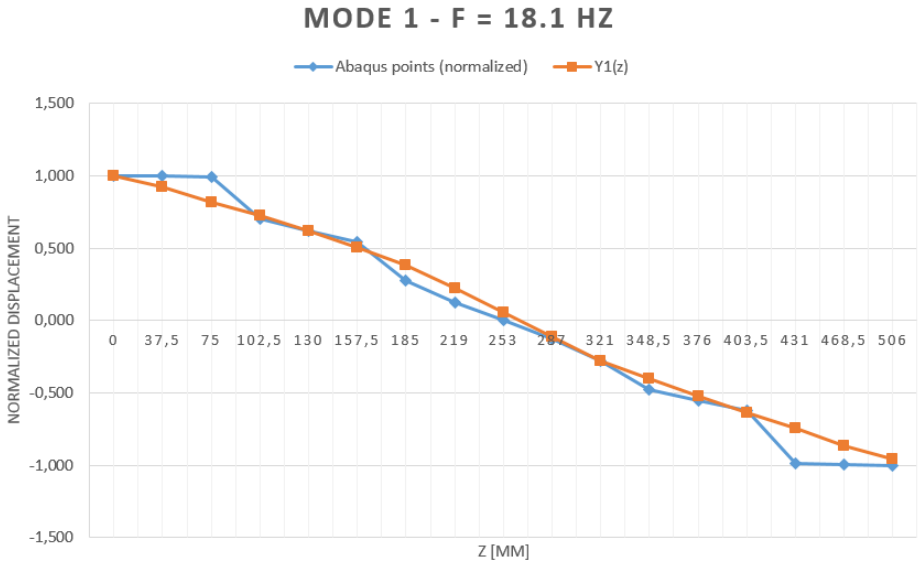

Figure 6.14: Plot of numerical values retrieved from Abaqus and the corresponding mode shape function $Y_1(z)$

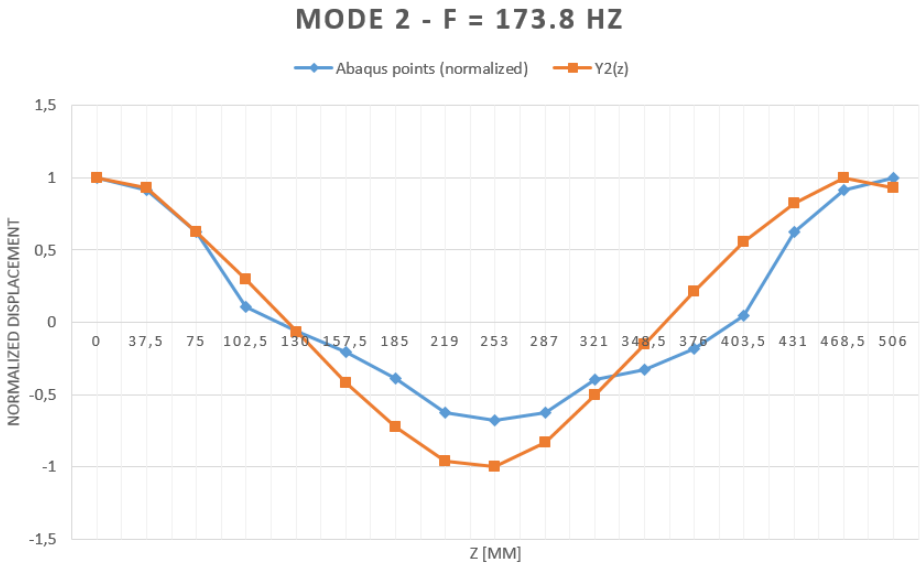

Figure 6.15: Plot of numerical values retrieved from Abaqus and the corresponding mode shape function $Y_2(z)$

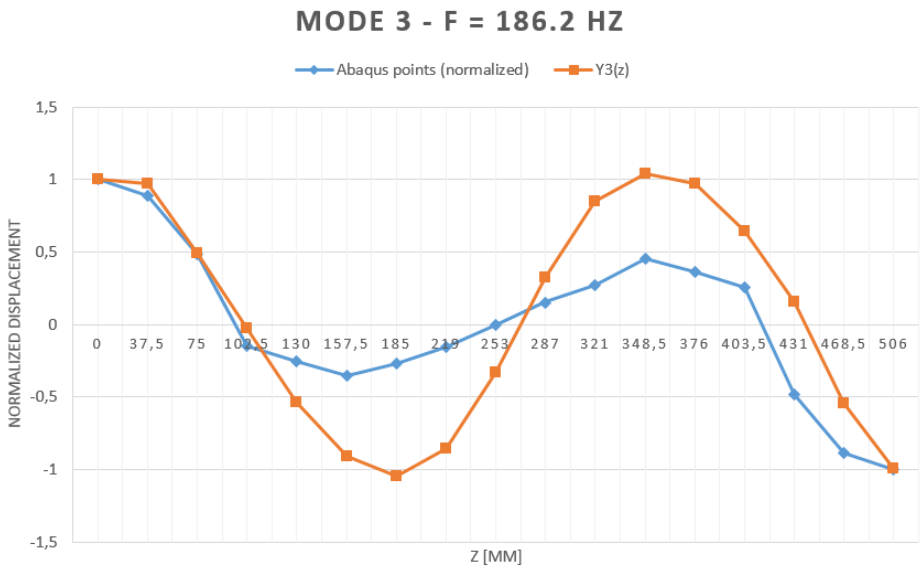

Figure 6.16: Plot of numerical values retrieved from Abaqus and the corresponding mode shape function $Y_3(z)$

In order to be able to use the method described in section 2.3, the mode shapes should be orthogonal. The condition for orthogonality is described in equation 2.3. Having obtained expressions for the three first mode shapes, the orthogonality can be checked:

$$\begin{aligned} \int_0^{506mm} Y_1(z) \cdot Y_2(z) &= -23.8 \\ \int_0^{506mm} Y_1(z) \cdot Y_3(z) &= 11.4 \\ \int_0^{506mm} Y_2(z) \cdot Y_3(z) &= 93.0 \end{aligned} \tag{6.9}$$

The mode shapes are not orthogonal. This result is discussed in section 7.2.2.

6.2.3 Frequency analysis – Case 2

The mode shapes yielded from the results in section 6.2.2 turned out to be non-orthogonal; see section 7. For that reason, another set of points were taken to attempt to get orthogonal mode shapes. This time, the selected nodes were all in the yz-plane, with all nodes taken along $x = 0$. The selected nodes are shown in figure 6.17. The boundary conditions were the same as in case 1.

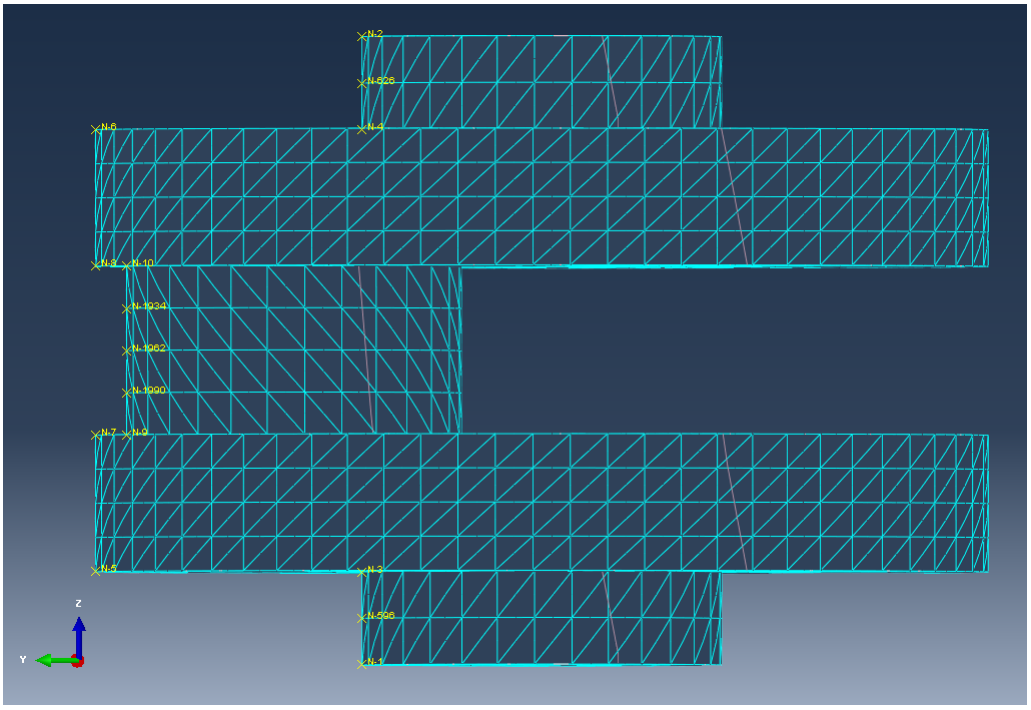

Figure 6.17: Illustration of nodes queried to retrieve mode shapes of the single crank

The same approach to retrieving the mode shape expressions as before was used. The selected values for retrieval of the mode shape expressions are shown in table 6.6.

Table 6.6: Selected values for retrieval of mode shape expressions along $x = 0$ (normalized)

Mode 1		**Mode 2**		**Mode 3**	
z [mm]	U_{norm}	**z [mm]**	U_{norm}	**z [mm]**	U_{norm}
0.0	1.000	0.0	1.000	0.0	1.000
219.0	0.432	185.0	-0.874	75.0	0.481
431.0	-0.953	468.5	0.916	321.0	0.529

The equation set 4.1 was again set up for each mode. For modes 1, 2 and 3, equations 6.10, 6.11 and 6.12 respectively were obtained:

$$\cos(431\alpha_1) + \frac{0.432 - \cos(219\alpha_1)}{\sin(219\alpha_1)} \sin(431\alpha_1) = -0.953 \tag{6.10}$$

$$\cos(468.5\alpha_2) + \left(\frac{-0.874 - \cos(185\alpha_2)}{\sin(185\alpha_2)}\right)\sin(468.5\alpha_2) = 0.916 \tag{6.11}$$

$$\cos(321\alpha_3) + \frac{0.481 - \cos(75\alpha_3)}{\sin(75\alpha_3)}\sin(321\alpha_3) = 0.529 \tag{6.12}$$

When solved for α_n ($n = 1,\ 2,\ 3$) using Newton's method, the following values were obtained:

- $B_1 = 0.394$
- $B_2 = -0.432$
- $B_3 = 0.427$
- $\alpha_1 = 0.0070$
- $\alpha_2 = 0.0113$
- $\alpha_3 = 0.0202$

In this case, the initial guess 0.02 was used to find α_3. For mode 1 and 2, an initial value of 0.01 was used. The expressions for the first three mode shapes (excluding the rigid body mode) were obtained:

$$\begin{aligned} Y_1(z) &= \cos(0.0070z) + 0.394\sin(0.0070z) \\ Y_2(z) &= \cos(0.0113z) - 0.432\sin(0.0113z) \\ Y_3(z) &= \cos(0.0202z) + 0.427\sin(0.0202z) \end{aligned} \tag{6.13}$$

Plots of the retrieved values from Abaqus vs. the corresponding mode shape functions are shown in figures 6.18, 6.19 and 6.20.

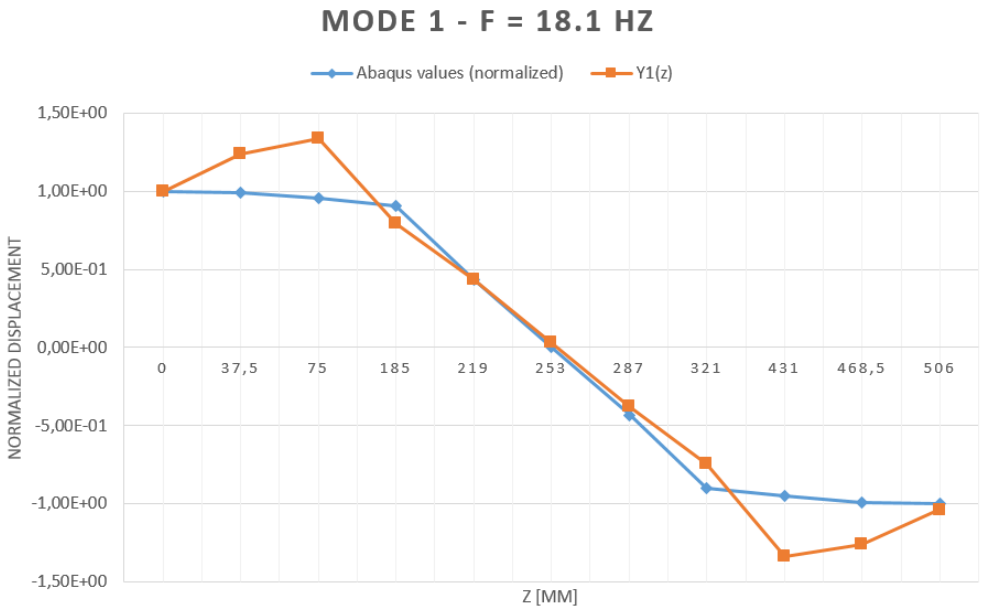

Figure 6.18: Plot of numerical values retrieved from Abaqus and the corresponding mode shape function $Y_1(z)$

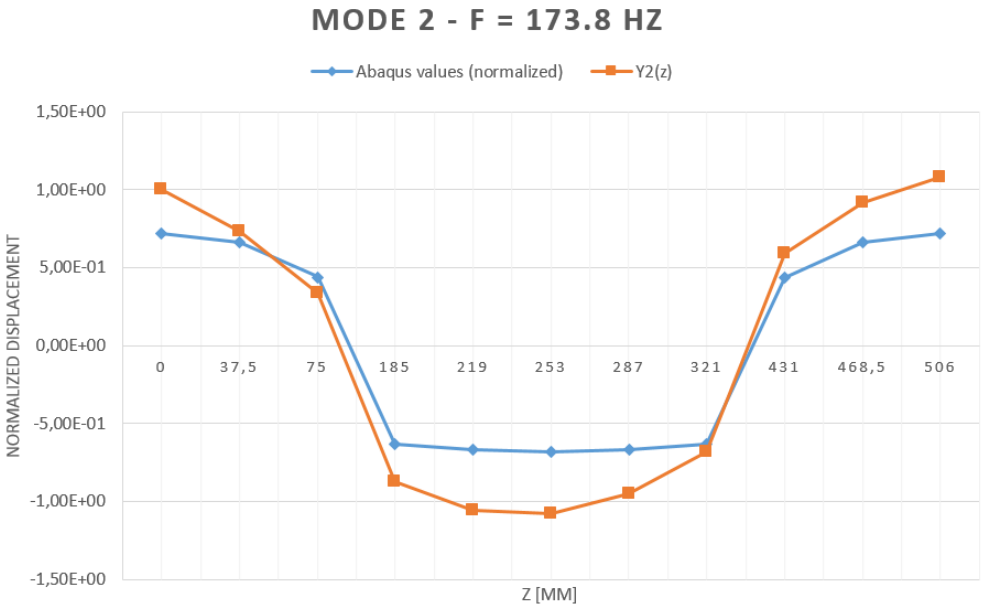

Figure 6.19: Plot of numerical values retrieved from Abaqus and the corresponding mode shape function $Y_2(z)$

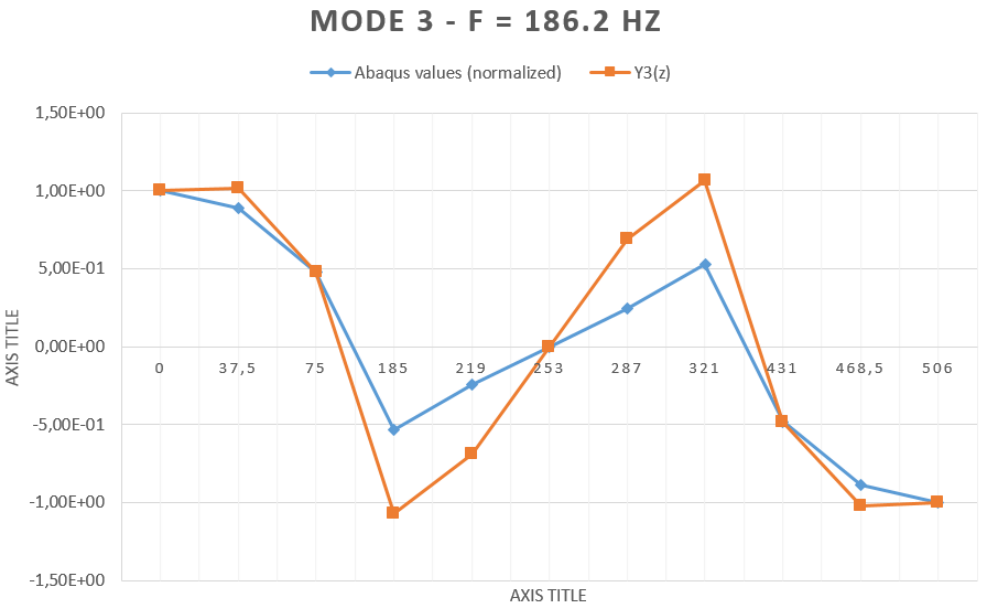

Figure 6.20: Plot of numerical values retrieved from Abaqus and the corresponding mode shape function $Y_3(z)$

Next, equation 2.3 was applied to the expressions in equation set 6.13 to check for orthogonality:

$$\begin{aligned} \int_0^{506mm} Y_1(z) \cdot Y_2(z) &= -67.7 \\ \int_0^{506mm} Y_1(z) \cdot Y_3(z) &= 41.0 \\ \int_0^{506mm} Y_2(z) \cdot Y_3(z) &= 8.6 \end{aligned} \tag{6.14}$$

The mode shapes are not orthogonal. This result is discussed in section 7.2.2.

CHAPTER 7

Conclusions and Discussion

In this section, the results from the Abaqus analyses will be discussed.

7.1 Simple cylinder

7.1.1 Inertia and stiffness

As shown in table 6.1, the mass moment of inertia about the z-axis, I_{zz}, given by Abaqus matched the analytical moment of inertia exactly.

The numerically calculated stiffness for mesh sizes 0.1 and 0.05 are also shown. Abaqus did not give the stiffness directly, but rather the value of the rotational displacement due to the applied torque. However, the error between the numerical and analytical result is the same for rotational displacement and stiffness, as both are scaled with the applied torque.

The difference in error when calculating the stiffness with different mesh sizes is worth noting. A finer mesh produces more accurate results at the expense of longer computational time. This increase in computational time is because the program has to solve more equations.

7.1.2 Frequency analysis

Table 6.2 shows that the analytical and numerical natural frequencies are well in agreement.

Though figure 6.2 looks like torsional mode 2, the frequency indicates that it is mode 1. As mentioned in section 6.1.2, the maximum displacement magnitude is 1 and the minimum is 0. The mode shape produced by Abaqus therefore seems to differ from the analytical result shown in figure 6.8, which has a range of -1 to 1. The reason for this is probably that Abaqus outputs magnitudes, i.e. an absolute value of the displacements.

It was, however, possible to determine which displacements were positive and negative by following the twist of the mesh lines along the z-axis. Using the right-hand rule, counter-clockwise twist along the z-axis means that the angular displacement is positive. Thus, clockwise twist along the z-axis will

give negative angular displacement. This method was not consistent for all modes, however. Using this approach on mode 3 would suggest that the value at $z = 0$ was -1, while it should be 1.

The B_n coefficients in equation 6.4 can be said to be approximately near zero. Further, the α_n constants are also very similar to their analytical counterparts, which are $\pi/10$, $2\pi/10$ and $3\pi/10$. This means that the resulting mode shape expressions match their analytical counterparts very well.

The results presented in section 6.1 show that the presented method of converting a set of numerically calculated modal displacements into mathematical expressions works well for a simple model such as a shaft. It is, however, unfortunate that the numerical modal displacements are given in absolute values.

7.2 Single crank

7.2.1 Inertia and stiffness

The numerical and analytical values for inertia are quite similar. The numerical result obtained from Abaqus only differs from the analytical result by about 0.15%.

As seen in table 6.4, the stiffness value calculated by Abaqus lies between the stiffness values calculated using Carter's and Ker Wilson's formulas. The validity of using Carter's (equation 3.14) and Ker Wilson's (3.15) formulas on the single crank finite element model is questionable. The overall shape of the crank is quite different from the one shown in figure 3.1. The discrepancies between the stiffness calculated by equations 3.14 and 3.15 and the numerical result could therefore arise as a result of this difference. Further, a more accurate numerical estimate of the stiffness could be obtained by using a finer mesh. However, Wilson (1956) notes that the average between his and Carter's formula can be used to determine the stiffness. If this is done, a stiffness of $K_{t,avg} = 9.0 \cdot 10^7 Nm/rad$ is obtained, which is quite close to the one given numerically by Abaqus.

Abaqus was well-suited to retrieve the inertia and stiffness of the models. Though the stiffness values was not used in this thesis, they could be used in a lumped parameter verification model. Material damping was not investigated in this work, but it is possible to include it when defining the material in an Abaqus model.

7.2.2 Frequency analysis

As seen in figure 6.14, the plots of the numerical displacements given by Abaqus and the mode shape function fit well. However, the plots for mode 2 and 3 show a larger spread of the values. This is true for both case 1 and case 2.

For each case, the displacements were sampled at the same nodes for all the modes. For each mode in case 2, the displacements sampled at the crank webs were disregarded, as they caused jumps in the plot. The displacement at a corresponding z-value on the main journal or crank pin was included instead. The overlapping nodes are shown in figure 6.17.

When selecting the three z-values for use in equation 6.8, it was found that some combinations would give an incorrect α-value. Attempts were made to set the initial guess close to the desired value, with no luck.

Different combinations of boundary conditions were applied to the single crank model in Abaqus. The intention was to isolate the torsional mode shapes, which turned out to be quite difficult. Modes which appeared to be non-torsional would normally be included, but they could be ruled out by using the "resultant vector" view, shown in figures 6.10, 6.11 and 6.12.

The results from Abaqus were given as displacement magnitudes. This is not believed to be a problem, as mode shapes are normally scaled in some way anyway (E. Pedersen, personal communication, January 6th, 2016). It was therefore not deemed necessary to spend time trying to convert the displacements to rotational displacements. One could also argue that the displacements are so small that they can be said to be approximately the same as the angle. However, this approximation only holds for a limited range of values before it becomes too inaccurate.

For the more complex single crank model, the method for retrieving mode shape expressions did not produce the desired results. As shown in section 6.2, the retrieved mode shape functions are not orthogonal. They can therefore not be used in the finite-mode bond graph models presented in 5.2. It is not certain that the retrieved mode shapes are incorrect even though the spread of values between the numerical and mathematical plots is large. It is also possible that the mathematical expression would fit the numerical points better if more than three points were used.

Because a lot of time was spent learning and working in Abaqus, and no usable mode shape expressions were obtained, no simulations of the bond

graphs were done. It can therefore not be stated whether the finite-mode representation of the crankshaft yields correct results.

CHAPTER 8

Suggestions for Further Work

A verification study to check if the retrieved mode shapes of the single crank model are correct should be carried out. It should also be checked whether or not it is possible to completely isolate the torsional modes in Abaqus. An attempt at this was made by using different combinations of boundary conditions, without much luck. It is not known whether certain combinations of boundary conditions affect the results of the frequency analysis, and if so, to what extent.

Another potential area of work is to find a better strategy for extracting the numerical displacements from which the mode shape expressions are obtained. One suggestion would be to connect the single crank throws together into a complete crankshaft and run a frequency analysis on the resulting model. The displacement values could then be collected along the crankshaft at, for example, the same point on each crank throw. Such a crankshaft model was made, but it could not be meshed due to a geometry error which arose when merging the single crank parts.

If verifiably correct mode shapes for the crankshaft are obtained, and if they are orthogonal, the finite-mode bond graph model should be verified through simulations. If it produces good results, it can potentially be connected to existing simulation models of a marine power train. This complete model can then be subjected to impulse loads from e.g. ice impact to see how it holds up compared to classical models.

References

Feese, T. and Hill, C. (2002). GUIDELINES FOR PREVENTING TORSIONAL VIBRATION PROBLEMS. In *Gas Machinery Conference*, volume 78249.

Friswell, M. I., Penny, J. E., Garvey, S. D., and Lees, A. W. (2012). *Dynamics of Rotating Machines*. Cambridge University Press, 1 edition.

Ginsberg, J. H. (1998). *Advanced Engineering Dynamics*. Cambridge University Press, 2 edition.

Huang, Y., Yang, S., Zhang, F., Zhao, C., Ling, Q., and Wang, H. (2012). Non-linear torsional vibration characteristics of an internal combustion engine crankshaft assembly. *Chinese Journal of Mechanical Engineering*, 25(4):797–808.

Irgens, F. (1999). *Formelsamling mekanikk*. Tapir.

Karnopp, D. C., Margolis, D. L., and Rosenberg, R. C. (2012). *System Dynamics : Modeling, Simulation, and Control of Mechatronic Systems*. Wiley, 5 edition.

Meirovitch, L. (1967). *Analytical Methods in Vibrations*. Macmillan, New York.

Mendes, A. S., Meirelles, P. S., and Zampieri, D. E. (2008). Analysis of torsional vibration in internal combustion engines : modelling and experimental validation. In *Proceedings of the Institution of Mechanical Engineers, Part K: Journal of Multi-body Dynamics*, pages 155–178.

Nestorides, E. (1958). *A handbook on torsional vibration*. University Press, Cambridge.

Pedersen, E. and Engja, H. (2010). *Mathematical Modelling and Simulation of Physical Systems*.

Pedersen, E. and Valland, H. (2014). *Lecture Notes in Mechanical Vibrations Courses TMR4222*.

Polić, D., Æsøy, V., and Ehlers, S. (2016). Transient simulation of the propulsion machinery system operating in ice - modeling approach. *Journal of Ocean Engineering Special Edition: Arctic Sea Transport (Submitted)*.

Rolls-Royce (2012). Diesel & gas engines.

Tiwari, R. (2010). *Analysis and Identification in Rotor-bearing Systems*. Department of Mechanical Engineering, IIT Guwahati, Guwahati, 1 edition.

Wakabayashi, K., Honda, Y., and Kodama, T. (1992). Dynamic characteristics of torsional viscous-friction dampers on reciprocal engine shafting. *SAE technical paper 921726*, pages 1–21.

Wilson, W. (1956). *Practical Solution of Torsional Vibration Problems vol. 1*. Chapman & Hall, London, 3 edition.

Appendices

A Numerical displacement magnitudes for the simple shaft

Table A.1: Numerical displacements for the simple shaft – Mode 1

z [m]	U_1
0.00	1.000
1.30	0.918
1.85	0.836
2.30	0.750
2.68	0.667
3.35	0.495
3.65	0.412
3.90	0.339
4.20	0.249
4.45	0.172
4.75	0.078
5.00	0.000
5.25	-0.078
5.55	-0.172
5.80	-0.249
6.10	-0.339
6.40	-0.426
6.70	-0.509
7.00	-0.588
7.35	-0.673
7.70	-0.750
8.15	-0.836
8.70	-0.918
10.00	-1.000

Table A.2: Numerical displacements for the simple shaft – Mode 2

z [m]	U_2
0.00	1.000
0.65	0.918
0.95	0.827
1.35	0.661
1.65	0.509
1.95	0.339
2.25	0.156
2.38	0.078
2.50	0.000
2.65	-0.094
2.75	-0.156
2.90	-0.249
3.20	-0.426
3.65	-0.661
3.85	-0.750
4.35	-0.918
5.05	-1.000
5.65	-0.918
6.15	-0.750
6.70	-0.482
7.03	-0.294
7.38	-0.078
7.50	0.000
7.60	0.063
7.75	0.156
8.05	0.339
8.20	0.426
8.50	0.588
9.05	0.827
9.35	0.918
10.00	1.000

Table A.3: Numerical displacements for the simple shaft – Mode 3

z [m]	U_3	**z [m]**	U_3
0.00	1.000	4.75	-0.233
0.65	0.818	4.90	-0.094
1.00	0.588	5.00	0.000
1.20	0.426	5.10	0.094
1.40	0.249	5.25	0.233
1.55	0.110	5.35	0.324
1.65	0.016	5.45	0.412
1.70	-0.031	5.55	0.495
1.75	-0.078	5.80	0.685
1.85	-0.172	6.05	0.836
1.95	-0.264	6.25	0.924
2.05	-0.353	6.70	1.000
2.20	-0.482	7.10	0.918
2.35	-0.600	7.45	0.740
2.45	-0.673	7.70	0.562
2.65	-0.800	7.90	0.397
2.90	-0.918	8.10	0.218
3.15	-0.985	8.25	0.078
3.35	-1.000	8.33	0.008
3.65	-0.956	8.50	-0.156
3.85	-0.884	8.80	-0.426
4.00	-0.809	9.00	-0.588
4.25	-0.649	9.25	-0.760
4.45	-0.495	9.50	-0.891
4.60	-0.368	10.00	-1.000

B Single crank mode shapes retrieved from Abaqus

Table B.1: Single crank: Case 1 – Mode 1

Node	**Location**	**z [mm]**	U_1	$U_{1,norm}$
18	Main journal	0.0	0.444	1.000
588	Main journal	37.5	0.443	0.998
76	Main journal	75.0	0.440	0.992
1233	Crank web	102.5	0.311	0.700
1171	Crank web	130.0	0.275	0.620
1109	Crank web	157.5	0.240	0.540
380	Crank pin	185.0	0.124	0.280
1984	Crank pin	219.0	0.056	0.126
1956	Crank pin	253.0	0.000	0.000
1928	Crank pin	287.0	-0.056	-0.126
423	Crank pin	321.0	-0.123	-0.277
1425	Crank web	348.5	-0.211	-0.476
1361	Crank web	376.0	-0.244	-0.550
1297	Crank web	403.5	-0.278	-0.626
119	Main journal	431.0	-0.440	-0.992
618	Main journal	468.5	-0.443	-0.998
61	Main journal	506.0	-0.444	-1.000

Table B.2: Single crank: Case 1 – Mode 2

Node	**Location**	**z [mm]**	U_2	$U_{2,norm}$
18	Main journal	0.0	0.892	1.000
588	Main journal	37.5	0.816	0.915
76	Main journal	75.0	0.558	0.626
1233	Crank web	102.5	0.096	0.108
1171	Crank web	130.0	-0.058	-0.065
1109	Crank web	157.5	-0.182	-0.203
380	Crank pin	185.0	-0.348	-0.391
1984	Crank pin	219.0	-0.555	-0.623
1956	Crank pin	253.0	-0.607	-0.681
1928	Crank pin	287.0	-0.555	-0.622
423	Crank pin	321.0	-0.353	-0.396
1425	Crank web	348.5	-0.294	-0.329
1361	Crank web	376.0	-0.161	-0.180
1297	Crank web	403.5	0.044	0.049
119	Main journal	431.0	0.559	0.626
618	Main journal	468.5	0.815	0.913
61	Main journal	506.0	0.891	0.999

Table B.3: Single crank: Case 1 – Mode 3

Node	**Location**	**z [mm]**	U_3	$U_{3,norm}$
18	Main journal	0.0	0.888	1.000
588	Main journal	37.5	0.787	0.887
76	Main journal	75.0	0.429	0.483
1233	Crank web	102.5	-0.134	-0.151
1171	Crank web	130.0	-0.226	-0.254
1109	Crank web	157.5	-0.314	-0.354
380	Crank pin	185.0	-0.240	-0.270
1984	Crank pin	219.0	-0.136	-0.153
1956	Crank pin	253.0	0.000	0.000
1928	Crank pin	287.0	0.136	0.153
423	Crank pin	321.0	0.239	0.270
1425	Crank web	348.5	0.402	0.453
1361	Crank web	376.0	0.323	0.364
1297	Crank web	403.5	0.228	0.257
119	Main journal	431.0	-0.428	-0.483
618	Main journal	468.5	-0.787	-0.887
61	Main journal	506.0	-0.888	-1.001

Table B.4: Single crank: Case 2 – Mode 1

Node	**Location**	**z [mm]**	U_1	$U_{1,norm}$
1	Main journal	0.0	0.098	1.000
596	Main journal	37.5	0.098	0.992
3	Main journal	75.0	0.094	0.953
9	Crank pin	185.0	0.089	0.906
1990	Crank pin	219.0	0.043	0.432
1962	Crank pin	253.0	0.000	0.000
1934	Crank pin	287.0	-0.042	-0.431
10	Crank pin	321.0	-0.089	-0.899
4	Main journal	431.0	-0.094	-0.953
626	Main journal	468.5	-0.098	-0.992
2	Main journal	506.0	-0.098	-1.000

Table B.5: Single crank: Case 2 – Mode 2

Node	**Location**	**z [mm]**	U_2	$U_{2,norm}$
1	Main journal	0.0	0.722	1.000
596	Main journal	37.5	0.662	0.916
3	Main journal	75.0	0.440	0.610
9	Crank pin	185.0	-0.631	-0.874
1990	Crank pin	219.0	-0.667	-0.924
1962	Crank pin	253.0	-0.684	-0.947
1934	Crank pin	287.0	-0.667	-0.924
10	Crank pin	321.0	-0.631	-0.874
4	Main journal	431.0	0.439	0.608
626	Main journal	468.5	0.662	0.916
2	Main journal	506.0	0.722	1.000

Table B.6: Single crank: Case 2 – Mode 3

Node	**Location**	**z [mm]**	U_3	$U_{3,norm}$
1	Main journal	0.0	1.000	1.000
596	Main journal	37.5	0.888	0.889
3	Main journal	75.0	0.481	0.481
9	Crank pin	185.0	-0.534	-0.534
1990	Crank pin	219.0	-0.245	-0.245
1962	Crank pin	253.0	0.000	0.000
1934	Crank pin	287.0	0.243	0.243
10	Crank pin	321.0	0.529	0.529
4	Main journal	431.0	-0.479	-0.479
626	Main journal	468.5	-0.889	-0.889
2	Main journal	506.0	-1.000	-1.000